

Surface Fitting Method Based on the
Boundary Curves of a Trimmed
Surface Considering the G^1 -continuity
with Adjacent Surfaces

Gulibaha Silayi

A thesis submitted for the degree of Doctor of Engineering

Department of Design and Media Technology
Graduate School of Engineering
Iwate University

September 2015

Abstract

A 3D CAD (Computer Aided Design) system is a system that can design a product shape in a three-dimensional model and it has become an indispensable tool for manufacturing. The 3D CAD system, which is the core of the application of Information Technologies, is spreading widely. 3D data designed with 3D CAD systems are becoming vital communication tools between the design process and downstream processes. The more extensive use of a 3D model outside traditional design and manufacturing is trending now. To distribute 3D data quickly to downstream departments is a significant boost to product quality, production costs, and delivery to markets. In the downstream department, 3D data received from a design department can be effectively utilized as a reference model for the creation of various process procedures and technical documents, such as creating visual assembly instructions, product manuals and product catalogs. In such works, clear visual communication for ease of understanding is important. However, size of 3D CAD data for expressing precise forms tends to be big and takes long time to compute, therefore it may interfere with communication among users. In addition, interoperability also causes poor communication since downstream applications rely on the reusability and interoperability of CAD models. Since the internal data structures and tolerances do not coincide in each system, the intended shape model for downstream distribution may not be delivered correctly. If the shape delivery fails in one system, the shape should be modified through some method to import suitably within the system. For example, the gap is one of the most serious interoperability challenges between CAD/CAM/CAE systems. To overcome the problem, the direct modeling which modifies the curve mesh is effective. In direct modeling, modification of a trimmed surface has the restriction where boundary edges must lie on the surface within a certain tolerance. Thus, it is difficult to maintain geometrical consistency of

the modified boundary edges and surfaces. Therefore, it is effective to apply a new free-form surface to a closed region enclosed with modified boundary edges because the consistency of the trimmed surface can be maintained.

In surface fitting method, how to guarantee a smooth connection between adjacent B-spline surfaces is very important. In conventional surface fitting method which approximates a surface using sample points derived from the tangent plane, the continuity with an adjacent surface will collapse because the surface was generated individually. In contrast, Muraki et al. proposed a surface fitting method in consideration of maintaining G^1 -continuity with adjacent surfaces. In their method, G^1 -continuity is guaranteed on part of the common boundary edges. However, when a surface connects with adjacent surfaces with G^1 -continuity in two adjoining directions along the common boundary edges, the conditions used as G^1 -continuous cannot be fulfilled near the corner portions with a B-spline surface.

The goal of this work is to make contribution to the communication among downstream processes using 3D data. To be more concrete, first we propose a new surface representation to solve the problems of the Muraki's method, then, contribute to the development of the current 3D data compression and retrieval method and evaluate the 3D data compression and retrieval application system. In our new surface fitting method, shapes can be approximated with good accuracy as a reference model for downstream processes. Our method generates a trimmed surface that is G^1 -continuous with adjacent surfaces in all directions and applicable to shapes with a hole. Our method integrates the advantages of Gregory and B-spline surfaces to define a new surface representation. First, when two surfaces are connected with G^1 -continuity, we calculate the G^1 -continuous control points at the common boundary by using joining equations. Next, a bi-cubic Gregory patch is constructed by the G^1 -continuous control points. Since the constructed Gregory patch is insufficient for representing a trimmed surface, knots are inserted in both u and v directions for increasing the degree of freedom. Then, the unknown inner control points are optimized using least squares approximation method. Finally, a new surface is constructed by applying our new surface representation to a closed region. The proposed method is applicable to shapes with a hole. Moreover, our method is independent of the position and the hole shape. Our method is also applicable to a region surrounded by surfaces in all directions connecting with G^1 -continuity. Since our method

generates surface from boundary edge information, it is applicable to various applications. For instance, by including our method in the trimmed surface compression method, a smooth surface with good quality can be generated. It is also effective for direct modeling where shapes with a hole are modified. Moreover, the performance of 3D data compression and retrieval application system is evaluated with different network environments: such as third generation of mobile telecommunications (3G) and Worldwide Interoperability for Microwave Access (WiMAX). As the result, we confirmed the effectiveness of the compression method with practical data.

Acknowledgements

First and foremost, my utmost gratitude to my Professor, Kouichi Konno, whose encouragement, guidance and support from the initial to the final level enabled me and inspired me as I hurdle all the obstacles in the completion of this research work. During times of doubt and depression, he would encourage and drag me along.

It is a pleasure to thank Professor Norishige Chiba, Professor Otsuka Naohiro, Associate Professor Tadahiro Fujimoto and Associate Professor Akashi Takuya for their valuable debates during the creation of this thesis.

I wish to thank Assistant Professor Katsutsugu Matsuyama, Assistant Professor Yuta Muraki and especially to Assistant Professor Tsutomu Kinoshita for their precious opinions, valuable comments and useful suggestions about this study. Additionally, I am also thankful to Mrs. Hikaru Kaketa for assistance with administrative work, Technical Staff Mrs. Kozue Shoji and Mr. Morimichi Furudate, whose helped improve research environment.

I would like to express my tremendous appreciation to the Rotary Yoneyama Memorial Foundation, especially Rotary International District 2520 Morioka South Rotary Club, for financially supporting me through my final one and a half years of my graduate school.

I also would like to make a special reference to LATTICE TECHNOLOGY, INC. for lending the modeling kernel.

It is with immense gratitude that I acknowledge the support and help of my family. Especially, my husband Aishajiang Rouziaji, my daughter Ainisha Aishajiang and my mother Zaorihan Rouzi. Without their unconditional love and endless support this thesis would not have been accomplished.

Lastly, I offer my regards and blessings to all the past and present members of Konno laboratory, those who supported me in any respect during the completion of this research.

List of Publications

Refereed Publications

- Gulibaha Silayi, Tsutomu Kinoshita, Yuta Muraki, Katsutsugu Matsuyama and Kouichi Konno, Evaluation of 3D Data Compression and Retrieval Method Based on Curve Mesh Filling. *Computer-Aided Design and Applications*, Vol.12, No.5, pp. 546-554, 2015.
- Gulibaha Silayi, Tsutomu Kinoshita, Katsutsugu Matsuyama and Kouichi Konno, Generating a Reference Model of the Surface with a Hole for Downstream Process. *Computer-Aided Design and Applications*, Accepted.

Contents

1	Introduction	1
1.1	Background	1
1.2	Motivations and Methodology	5
1.3	Thesis outline	6
2	Related Works	7
2.1	Methods Based on the Surface Interpolation Method	7
2.2	Methods Based on the N-side Filling Method	9
2.3	Surface Fitting Method with G^1 -Continuity	11
2.4	Problems of Related Works	13
3	New Surface Fitting Method	15
3.1	Introduction	15
3.2	Background	15
3.3	New Surface Representation	16
3.4	Joining With the Adjacent Surface	19
3.5	Approximation	21
3.5.1	Approximation Process	21
3.6	Evaluation of Generated Surface	23
3.7	Experimental Results	23
3.8	Summary	37
4	3D Data Compression and Retrieval Application	38
4.1	Introduction	38
4.2	Background	38
4.3	Surface Compression Method	40

4.3.1	Concept of Surface Compression Method	40
4.3.2	Compression Part	41
4.3.3	Flow Chart of Data Compression Part	42
4.4	Surface Retrieval Method	44
4.4.1	Retrieval Part	44
4.5	Experimental Results	50
4.6	Performance Evaluation Method	50
4.6.1	Evaluation Result by Success Rate	55
4.6.2	Evaluation Result by Data Size	55
4.6.3	Evaluation Result by Data Transmission Time	58
4.7	Summary	61
5	Conclusion and Future Work	65
5.1	Conclusion	65
5.2	Future Work	66
A	Derivation of the joining equations	68
B	Surface inner control point calculation by least-squares approximation method	70
	Bibliography	74

Chapter 1

Introduction

1.1 Background

A 3D CAD (Computer Aided Design) system, is a system that can design a product shape in the three-dimensional model and it has become an indispensable tool for manufacturing. Manufacturing has been globalized during the last two decades. Designed and manufactured by the manufacturing facilities around the world have been routinely performed. From a manufacturer's perspective, a 3D model is beneficial information because it allows visualization of exactly what the finished product being made will look like. This can be particularly helpful when dealing with complex geometries that difficult to interpret from a 2D drawing alone. Since the 3D CAD system, is defined the use of information technology (IT) in the design process. The 3D model designed with 3D CAD systems are becoming vital communication tools between the design process and downstream processes. As shown in Figure 1.1, use of 3D models in downstream processes can be classified in following two categories:

- 3D models on the critical path.
- 3D models off the critical path.

The '3D models on the critical path' indicates the use release of 3D models from engineering to the manufacturing organization, where the 3D models are then used for production purposes. The '3D models off the critical path'

indicates the use release of 3D models outside the hand off between engineering and manufacturing, such as: 3D models in service, quality, training, technical documentation, marketing, sales and other organizations [1].

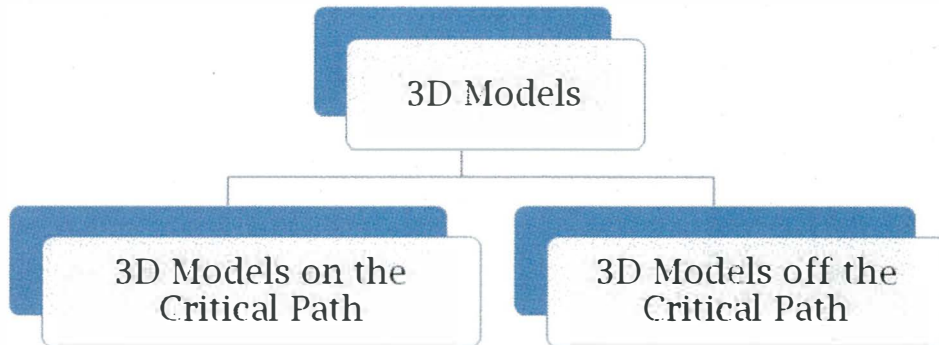


Figure 1.1: The use of 3D Models in downstream processes.

Figure 1.2 illustrates the use of 3D Models off the critical path. According to the recent reports, the use of 3D models in downstream processes is significantly growing in the past few years, approximately 69% of companies are using 3D models off the critical path [1]. On one hand, use of 3D on the critical path requires the level of precision to manufacture since it is for the production purposes. On the other hand, use of 3D off the critical path requires the visual impact rather than precision since 3D data designed with 3D CAD systems utilized as a reference model in many CAD Viewers. CAD Viewer is a type of software used to perform various derivative tasks with 3D Models throughout the product life cycle, but does not create them [1]. This paper studies the obstacles of the communication between the downstream processes using the 3D CAD models designed with 3D CAD systems. Our main focus is the use of 3D models off the critical path in downstream processes.

Quickly distributing 3D data to downstream departments can dramatically enhance their work efficiency. In the downstream department, a 3D model received from a design department can be effectively utilized as a reference model for the creation of various process procedures and technical documents, such as creating visual assembly instructions, creating product manuals and product catalogs. In such works, clear visual communication for ease of understanding is important. However, since the internal data structures and tolerances do not coincide in each system, the intended shape model for

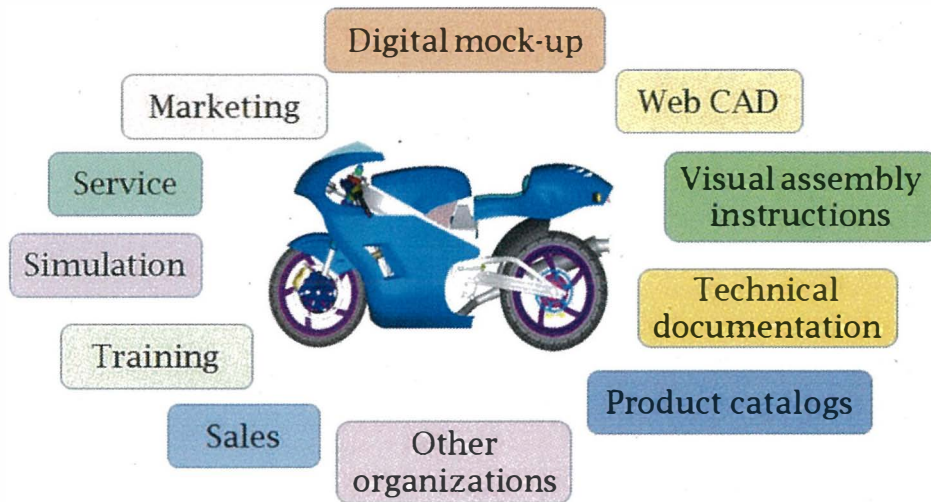


Figure 1.2: 3D Models use off the critical path.

downstream distribution may not be delivered correctly. If the shape delivery fails in one system, the shape should be modified through some method to import suitably within the system. To overcome the problem, the direct modeling which modifies the curve mesh is effective. For example, Figure 1.3 shows the gap between two trimmed surfaces which was caused by the different tolerances. The gap is one of the most serious interoperability challenges between CAD/CAM/CAE systems [2].

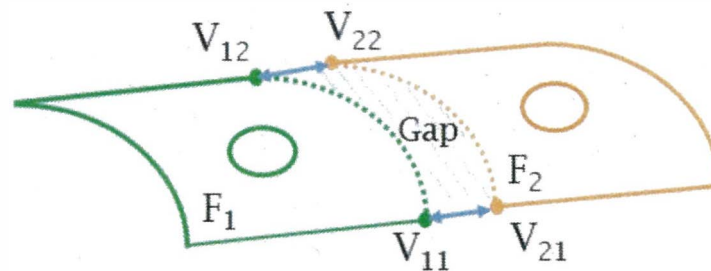


Figure 1.3: Modifying a boundary edge in direct modeling for data healing.

In direct modeling, modification of a trimmed surface [3] has the restriction where boundary edges must lie on the surface within a certain tolerance. Thus, it is difficult to maintain geometrical consistency of the modified boundary edges and surfaces. Therefore, it is effective to apply a new free-form surface

to a closed region enclosed with modified boundary edges because the consistency of the trimmed surface can be maintained. Since downstream processes concern surface smoothness rather than the precision of the approximated surface, the smoothness is more important than the approximation precision. Because, 3D surface models show the entire 3D image and shape of an object, so the visual impact is more important. For instance, Figure 1.4 illustrates the importance of the visible connections between surfaces of two same 3D objects. At a first glance, we can see that which one is more appropriate as a reference model. In consideration of the discontinuity at connection parts as marked in red circles in Figure 1.4(b), Figure 1.4(a) is more appropriate than Figure 1.4(b) as a reference model.

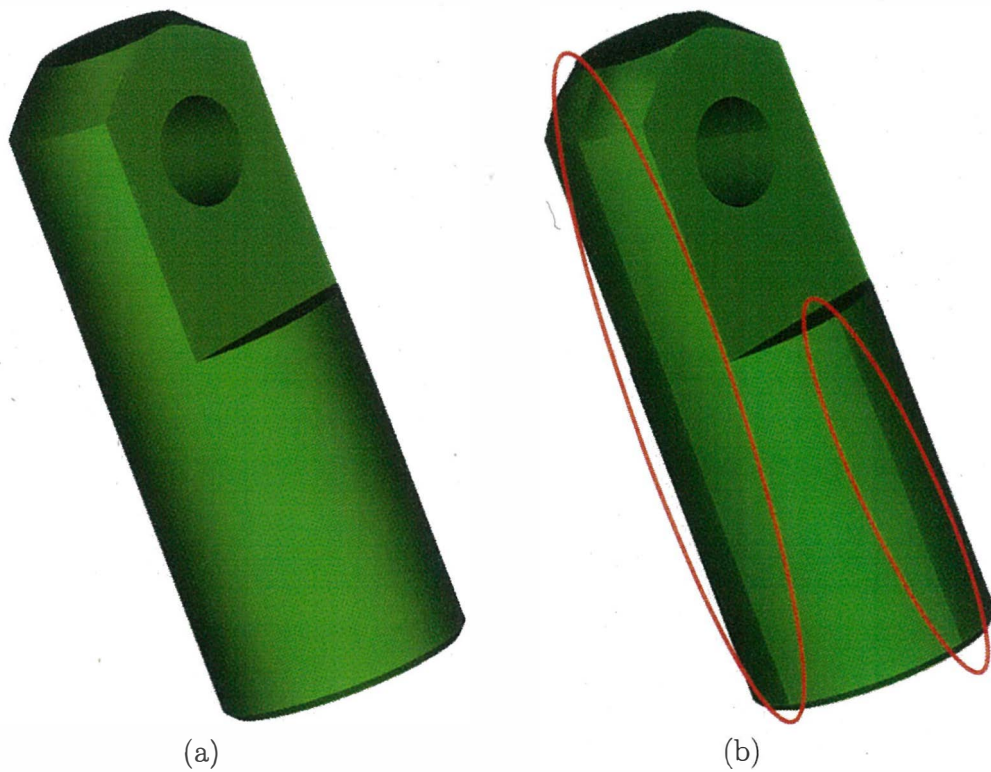


Figure 1.4: Example of surface smoothness.

The problem of smooth connection will reduce the quality of the data as a reference model. In conventional surface fitting method which approximates a surface using sample points derived from the tangent plane, the continuity

with an adjacent surface will collapse because the surface was generated individually. In contrast, the surface fitting method [7] is proposed by Muraki et al. in consideration of maintaining G^1 -continuity with adjacent surfaces. In their method, G^1 -continuity is guaranteed on the common boundary edges. However, when a surface connects with adjacent surfaces with G^1 -continuity in two adjoining directions along the common boundary edges, the conditions used as G^1 -continuous cannot be fulfilled near the corner portions with a B-spline surface. In Figure 2.1(a), the red x marks are indicate the discontinuous portion near the corner of the common boundary edges. Therefore, in this thesis we proposed a new surface fitting method based on the boundary curves of the trimmed surface considering the G^1 -continuity with adjacent surfaces.

In addition, size of 3D CAD data for expressing precise forms tends to be big and takes long time to compute, therefore it may interfere with communication among users. To distribute 3D data quickly to downstream departments is significant boosts to product quality, production costs, and delivery to markets. As a result, 3D data compression and retrieval algorithm is required to easily exchange such information through the Internet.

Therefore, our contribution to the communication among downstream processes using 3D data can be summarized as follow:

1. Propose a new surface fitting method based on the boundary curves of the trimmed surface considering the G^1 -continuity with adjacent surfaces.
2. Contribute to the development of the current 3D data compression and retrieval method and evaluated the 3D data compression and retrieval application system.

1.2 Motivations and Methodology

The goal of this work is to make contribution to the communication among downstream processes using 3D data. To be more concrete, propose a new surface representation to solve the problems of the Muraki ' s method first. Then, contribute to the development of the current 3D data compression and retrieval method and evaluate the 3D data compression and retrieval application system. In our new surface fitting method, shapes can be approximated

in good accuracy as a reference model for downstream processes. Our method generates a trimmed surface that is G^1 -continuous with adjacent surfaces in all directions and applicable to shapes with a hole. Moreover, the performance of 3D data compression and retrieval application system is evaluated with different network environments: such as third generation of mobile telecommunications (3G) and Worldwide Interoperability for Microwave Access (WiMAX). As the result, we confirmed the effectiveness of the compression method with practical data.

1.3 Thesis outline

This thesis is composed of 5 chapters including this chapter and each chapter is composed with several sections. Outline of each chapter is organized as follows.

- Chapter 1 introduces the background of communication among downstream processes using 3D models and a brief introduction of our main contribution.
- Chapter 2 describes the related works and their problems. Surface interpolation, N-side filling and surface fitting with G^1 -continuity are described as our related works. We also discussed the problems of related works.
- Chapter 3 presents the new surface fitting method based on the boundary curves of the trimmed surface considering the G^1 -continuity with adjacent surfaces. Then the practicality of our method is evaluated by applying it to the practical CAD data and practicality is verified with shapes with a hole.
- Chapter 4 introduces the evaluation of 3D data compression and retrieval application. The performance of 3D data compression and retrieval application system is evaluated with different network environments: such as third generation of mobile telecommunications (3G) and Worldwide Interoperability for Microwave Access (WiMAX).
- Finally, we conclude this thesis in Chapter 5.

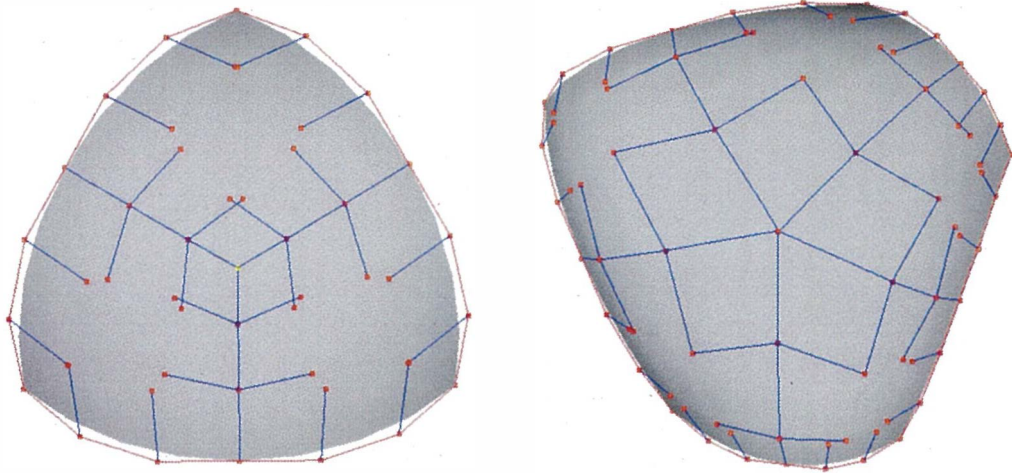
Chapter 2

Related Works

2.1 Methods Based on the Surface Interpolation Method

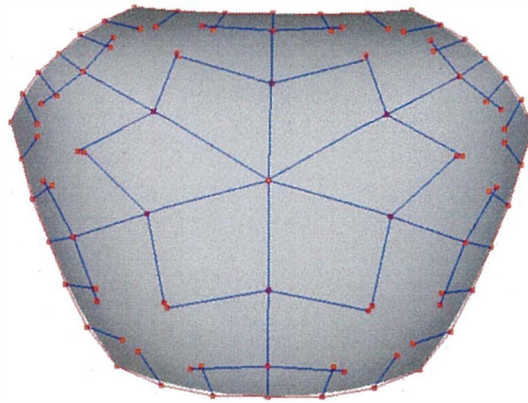
The surface interpolation method is a method that generates a surface inside an area bounded by edges. In general, a four-sided area is interpolated with one surface. An N-sided area except for four-sided is interpolated with two or more surface patches. The inner curves are generated based on Catmull-Clark subdivision [8] and the N-sided region is divided into N quadrilateral regions. Then, a surface is interpolated to each of the generated regions. For example, Figure 2.1 shows the control points of an N-sided area that generated based on Catmull-Clark subdivision method. In Figure 2.1(a), three-sided area divided into 3 quadrilateral regions. In Figure 2.1(b), five-sided area divided into 5 quadrilateral regions and six-sided area divided into 6 quadrilateral regions in Figure 2.1(c). Each of the quadrilateral regions is smoothly interpolated with a Gregory patch. Therefore, in the surface interpolation method, each patch can be connected with G^1 -continuity. Piegl et al. introduced an interpolation method with the angle tolerance ϵ to generate smooth surfaces [9]. In his method, it is possible to control the continuity between patches with the control points for connecting them between patches that are computed by the cross-boundary derivative. Yang et al. enhanced the Piegl's method to apply it to rational curve meshes [10]. In other research, Garcia et al. proposed the

surface interpolation method of an arbitrary N-sided region by dividing the region into a star-shaped N-sided patch and quadrilateral patches. The size of the star-shaped N-sided patch can be controlled using parameter f . If the value of f increases, the N-sided region will be larger; and if the value of f decreases, the region will be smaller [11].



(a) Three-sided area

(b) Five-sided area



(c) Six-sided area

Figure 2.1: Example of surface interpolation method application to the N-sided area.

2.2 Methods Based on the N-side Filling Method

Tokuyama et al. proposed an N-side filling method [15] that covers an N-sided region with a B-spline surface. His method is the one that calculates the control points of the B-spline surface by using only the boundary edges of the surface. Since his technique is a basis of surface fitting research, a concrete procedure is described below:

1. Suppose a surface is applied to a closed region whose boundary edges are drawn in blue in Figure 2.2(a). First, as shown in Figure 2.2(a), four reference planes are generated outside of the closed region.
2. As shown in Figure 2.2(b), the cross boundary derivatives are extended to the outside of the closed region, and the intersection points with four reference planes are generated.
3. As shown by the purple lines of Figure 2.2(c), the intersection point sets generated in Step.2 are approximated with B-spline curve, and the boundary curves that cover an N-sided region are generated.
4. As shown by the purple points of Figure 2.2(d), the sample points are generated on the lines that generated in Step.2.
5. As shown in Figure 2.2(e), the control points of the B-spline surface are derived from the boundary curves generated in Step.3 and the sample points generated in Step.4 by using the least-squares method.

The Tokuyama's method, however, is not applicable to concave shapes. Therefore, Muraki et al. [12] enhanced the N-side filling method for applying it to the shapes with holes or concave shapes and to maintain G^1 -continuity with adjacent surfaces in only one direction [5, 6].

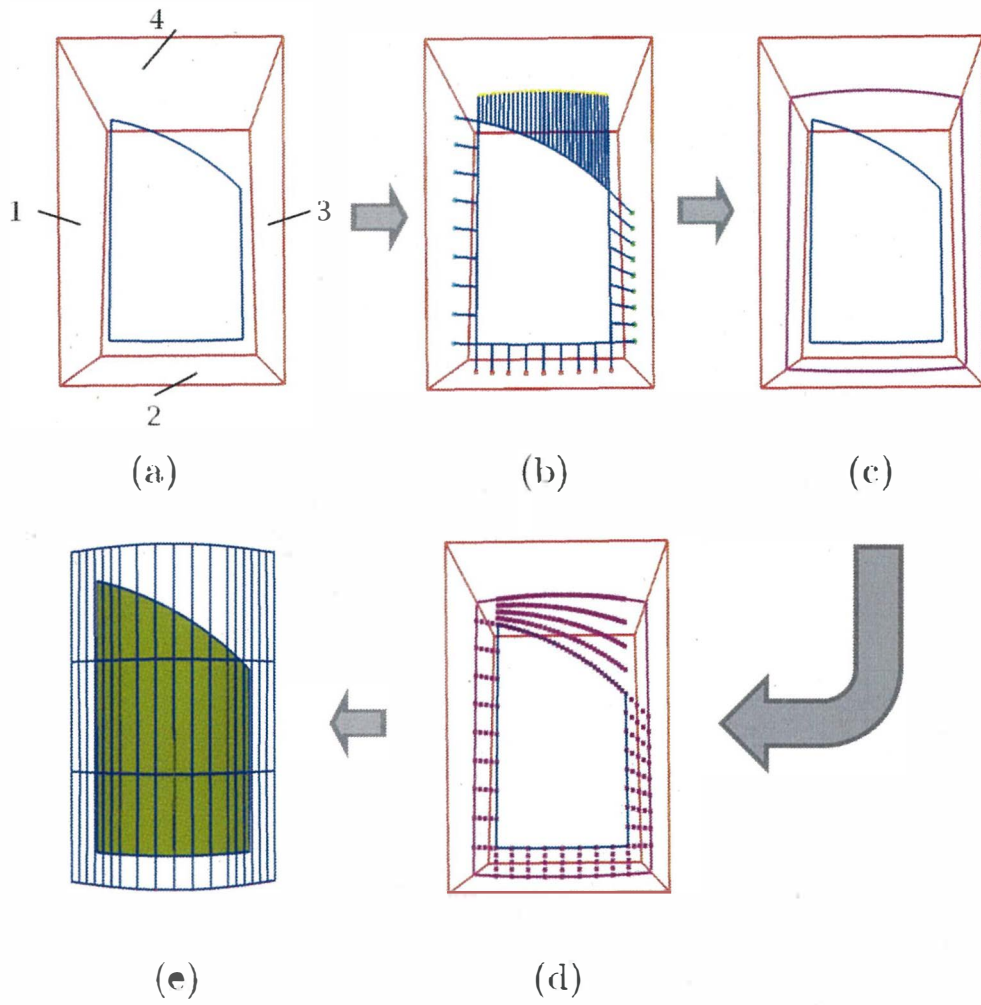
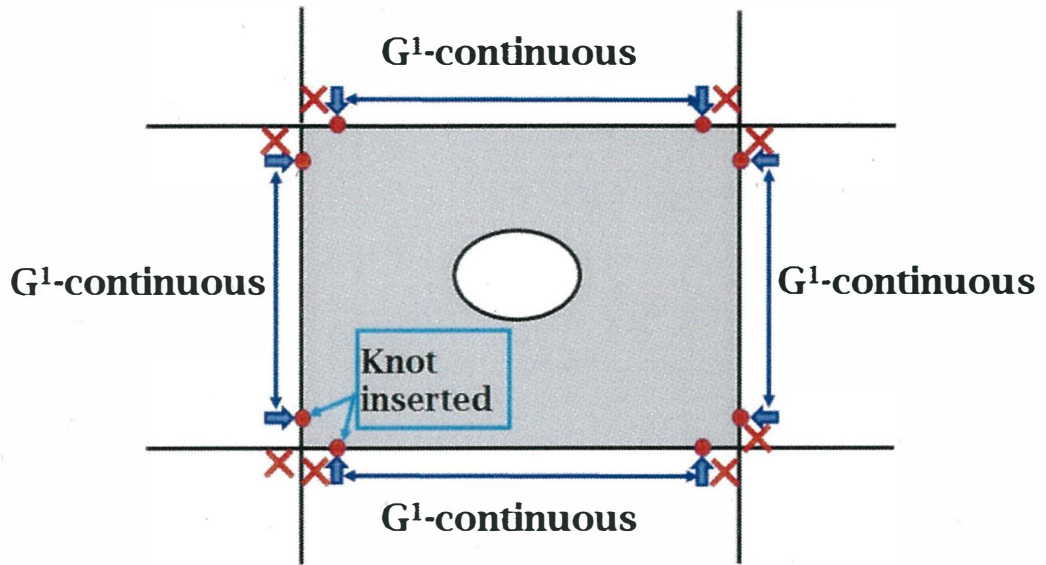


Figure 2.2: The procedure of the N-side filling method.

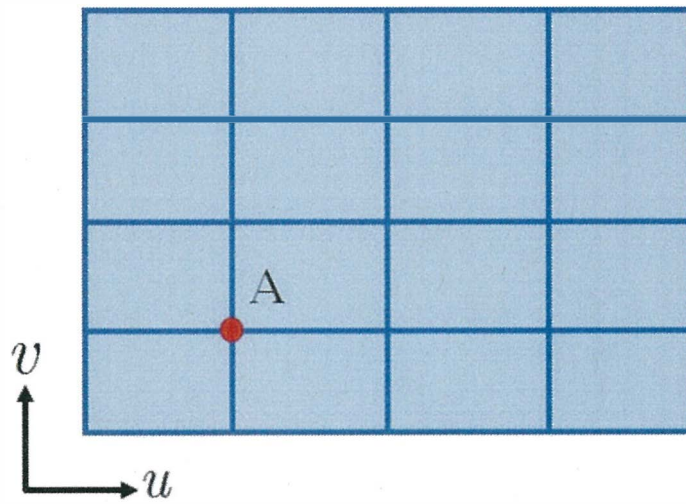
2.3 Surface Fitting Method with G^1 -Continuity

In the field of CAD, construction of N-side region has received a lot of attention. Especially, generating a smooth surface with adjacent surface approaches are developed in the past few years. Since with the N-side filling method described in the section 2.2 cannot generate a smooth surface with adjacent surfaces, Muraki et al. [5, 6] enhanced the N-side filling method for apply it to the shapes with holes or concave shapes and to maintain G^1 -continuity with adjacent surfaces in one direction. Moreover, the method [5, 6] realizes connection with an adjacent surface with G^1 -continuity in only one direction. If, however, the number of the boundary edges connected with adjacent surfaces with G^1 -continuity increases, the number of the sample points will decrease, and the control points will be unstable. Therefore, Muraki et al. enhanced [5, 6] and proposed a reconstruction method of trimmed surfaces for an N-side region and allowed discontinuous portions near the corners of the common boundary edges [7]. In Figure 2.1(a), the red x marks are indicate the discontinuous portion near the corner of the common boundary edges. His method unites the advantages of the surface interpolation method [22, 26] and the N-side filling method [9]. On a common boundary where two surfaces should be connected with G^1 -continuity, an input curve mesh is represented by cubic Bézier curves and the cross boundary derivatives are calculated based on the basis patch method [26]. Among control points of the B-spline surface, the control points lying on the inner side of the boundary curves are calculated by the surface interpolation method. Moreover, other internal control points are calculated by the N-side Filling method.

However, by using conventional B-spline surfaces, the cross-boundary derivative vectors cannot be specified independently. Concretely, as shown in Figure 2.3(b), the control point ‘A’ indicates the only control point that involves in calculation of a B-spline surface cross-boundary derivatives in u and v directions. Therefore, when the connection with adjacent surfaces performed successively in u and v directions, B-spline has no degree of freedom to individually define the connections of two surfaces with G^1 -continuity in u and v directions. Moreover, when a surface connects with adjacent surfaces in two adjoining directions along common boundary edges as shown in Figure 2.3(a), knots are inserted near the corners (at parameters 0.05 and 0.95) [7] in order to narrow down the discontinuous section with the adjacent surfaces even if



(a)



(b)

Figure 2.3: Problems of the method of Muraki et al.[7].

two surfaces have to be connected with G^1 -continuity. However, the method of determining the knot values near the corners are unclear.

In surface reconstruction, how to guarantee a smooth connection between adjacent B-spline surfaces, is very important. Mu et al. proposed the construction of B-spline surfaces by interpolating its boundary curves, or even the cross-boundary derivatives, and the inner points were approximated simultaneously [16]. In their method, a B-spline surface is smoothly connected with adjacent surfaces, however, it cannot be respond to local modification and the applicability to the shapes with a hole was not discussed in the literature.

2.4 Problems of Related Works

This section describes problems of related works that explained earlier. The advantages and disadvantages of the related works are summarized as follow:

- As described in section 2.1, the methods based on the surface interpolation method [9, 11, 26] are excellent in continuity with adjacent surfaces. The methods [9, 11, 26] consider the continuity between two or more surface patches. However, since these methods divide an N-sided region into two or more regions, it is inapplicable to the shapes with holes or concave shapes. Also, the methods are dependent on the shapes of the boundary edges expressing a closed region, and the division of concave shapes may fail. Since notches appear frequently in the machine parts include shapes with holes or concave shapes are expressed with trimmed surfaces, it is difficult to apply the surface interpolation method.
- As described in section 2.2, among the methods based on the n-side filling method: the Tokuyama's method [15] is inapplicable to the shapes with hole or concave shapes. Also, the connection between adjacent surfaces is not considered. Although, the method [12] can be applicable to the shapes with hole or concave shapes. However, also the continuity with adjacent surfaces is not maintained. In contrast, the method [5, 6] can be applicable to the shapes with hole or concave shapes and also G^1 -continuous with adjacent surfaces in only one direction.

- As described in section 2.3, the method of Muraki et al. [7] unites the advantages of the surface interpolation method [22, 26] and the N-side filling method [9]. However, when a surface connects with adjacent surfaces in two or more adjoining directions along common boundary edges, their method allowed discontinuous portions near the corners of the common boundary edges. Moreover, although the method of Mu et al. [16] succeeded in generating a smooth B-spline surface with adjacent surfaces, however, it cannot be respond to local modification and the applicability to the shapes with a hole was not discussed in the literature.

In surface reconstruction, how to guarantee a smooth connection between adjacent B-spline surfaces, is very important. If the normal vectors around the corner area do not coincide with each other, contradiction occurs in the geometric calculation of the surface. Discontinuity of the shapes that are suppose to be G^1 -continuous will lowers shape data quality as a reference model, because users are expected to see the exact designed shape. For instance, when various evaluation procedures performed to the shape models, such as extraction of continuous surfaces and generation of cross section, curve sequence of cross section becomes discontinuous at junctions. Therefore, we mainly focused on the problems of Muraki et al. and propose a new surface fitting method. Concretely, a new surface representation with which the cross-boundary derivatives can be specified independently in both u and v directions with the B-spline blending functions proposed first. Then, the practicality of our method is evaluated by applying it to the practical CAD data. More details of our approach will be discussed in the next chapter.

Chapter 3

New Surface Fitting Method

3.1 Introduction

In surface reconstruction, how to guarantee a smooth connection between adjacent B-spline surfaces, is very important task. As described in chapter 2, surface fitting methods have their problems to solve. In this chapter we significantly focused on the problems of the related works described in section 2.3. Therefore, this chapter describes a new surface fitting method based on the boundary curves of the trimmed surface with considering the G^1 -continuity with adjacent surfaces. Then, the practicality of our method is evaluated by applying it to the practical CAD data and practicality is verified with shapes with a hole.

3.2 Background

The value of 3D CAD models is continuously increasing in downstream processes. The more extensive use of a 3D model outside traditional design and manufacturing is trending now. To distribute 3D data quickly to downstream departments is significant boosts to product quality, production costs, and delivery to markets. Unfortunately, interoperability causes poor communication since downstream applications rely on the reusability and interoperability of CAD models. However, 3D CAD data size for expressing precise

forms tends to be big and time-consuming for computation, which may interfere in the communication. In addition, downstream processes emphasize surface smoothness more than precision. Therefore, this thesis describes the reconstruction method of a smooth surface by integrating the advantages of Gregory and B-spline surfaces. In our approach, a new surface representation is proposed. Two surfaces are connected with G^1 -continuity by using the control points at the common boundary obtained from joining equations. The internal control point that is not connected to the boundary curve is obtained from the least squares approximation method. The proposed method is applicable to shapes with a hole.

3.3 New Surface Representation

As described in section 2.3, since when the connection with adjacent surfaces performed successively in u and v directions, B-spline surface has no degree of freedom to individually define the connections of two surfaces with G^1 -continuity in u and v directions. A new surface representation with which the cross-boundary derivatives can be specified independently in both u and v directions with the B-spline blending functions proposed. This research integrates the advantages of the B-spline and Gregory surfaces to define a new surface representation. To be more concrete, construction of a new surface representation via the boundary curves and approximation of the inner control points will be studied. We express a fitting surface $\mathbf{S}(u, v)$ using surface control points $\mathbf{P}_{i,j,k}$ ($i = 0, \dots, n, j = 0, \dots, m, k = 0, 1$). Surface $\mathbf{S}(u, v)$ is expressed by Equation (3.1), where $N_i^3(u)$ and $N_j^3(v)$ are the cubic B-spline basis functions over the knot spans $\mathbf{U} = [0, 0, 0, 0, u_0, \dots, u_p, 1, 1, 1, 1]$ and $\mathbf{V} = [0, 0, 0, 0, v_0, \dots, v_q, 1, 1, 1, 1]$.

$$\mathbf{S}(u, v) = \sum_{i=0}^3 \sum_{j=0}^3 N_i^3(u) N_j^3(v) \mathbf{Q}_{ij}(u, v) \quad (3.1)$$

The rational functions \mathbf{Q}_{ij} ($0 \leq i \leq n, 0 \leq j \leq m$) are defined by the following relationships:

1. If $(i, j) = (1, 1), (1, m - 1), (n - 1, 1), (n - 1, m - 1)$, then

$$\mathbf{Q}_{1,1}(u, v) = \frac{u\mathbf{P}_{110} + v\mathbf{P}_{111}}{u + v} \quad (0 \leq u \leq u_0, 0 \leq v \leq v_0) \quad (3.2)$$

$$\mathbf{Q}_{1,m-1}(u, v) = \frac{u\mathbf{P}_{1,(m-1),0} + (1-v)\mathbf{P}_{1,(m-1),1}}{u + (1-v)} \quad (0 \leq u \leq u_0, v_q \leq v \leq 1) \quad (3.3)$$

$$\mathbf{Q}_{n-1,1}(u, v) = \frac{(1-u)\mathbf{P}_{(n-1),1,0} + v\mathbf{P}_{(n-1),1,1}}{(1-u) + v} \quad (u_p \leq u \leq 1, 0 \leq v \leq v_0) \quad (3.4)$$

$$\mathbf{Q}_{n-1,m-1}(u, v) = \frac{(1-u)\mathbf{P}_{(n-1),(m-1),0} + (1-v)\mathbf{P}_{(n-1),(m-1),1}}{(1-u) + (1-v)} \quad (u_p \leq u \leq 1, v_q \leq v \leq 1) \quad (3.5)$$

2. If others, then

$$\mathbf{Q}_{i,j} = \mathbf{P}_{i,j,0} \quad (3.6)$$

In our method, a surface is fitted using the Equation (3.1), and the concept of our method is shown in Figure 3.1. Figure 3.1(a) shows surface F that has G^1 -continuous adjacent surfaces F_1 , F_2 , F_3 and F_4 in all four directions with a hole. On a common boundary where two surfaces are connected with G^1 -continuity, each boundary of an input curve mesh is represented by a cubic Bézier curve. The concept of our proposed method explains in the case where knots are inserted at parameters $u_0 = 0.5$ and $v_0 = 0.5$ ($p = 0, q = 0$) as shown in Figure 3.1(b). The yellow control points are obtained from boundary curves, the red ones are obtained by the joining equations [14] and the blue one is obtained by the least squares approximation method.

The flow of our surface fitting procedure are described as below:

- First, when two surfaces are connected with G^1 -continuity, we calculate the G^1 -continuous control points at the common boundary by using joining equations described in section 3.4.
- Next, a bi-cubic Gregory patch is constructed by the G^1 -continuous control points. Since the constructed Gregory patch is insufficient for representing a trimmed surface, knots are inserted in both u and v directions for increasing the degree of freedom.
- Then, the unknown inner control points are optimized using the least squares approximation method [21].
- Finally, a new surface is constructed using Equation (3.1).

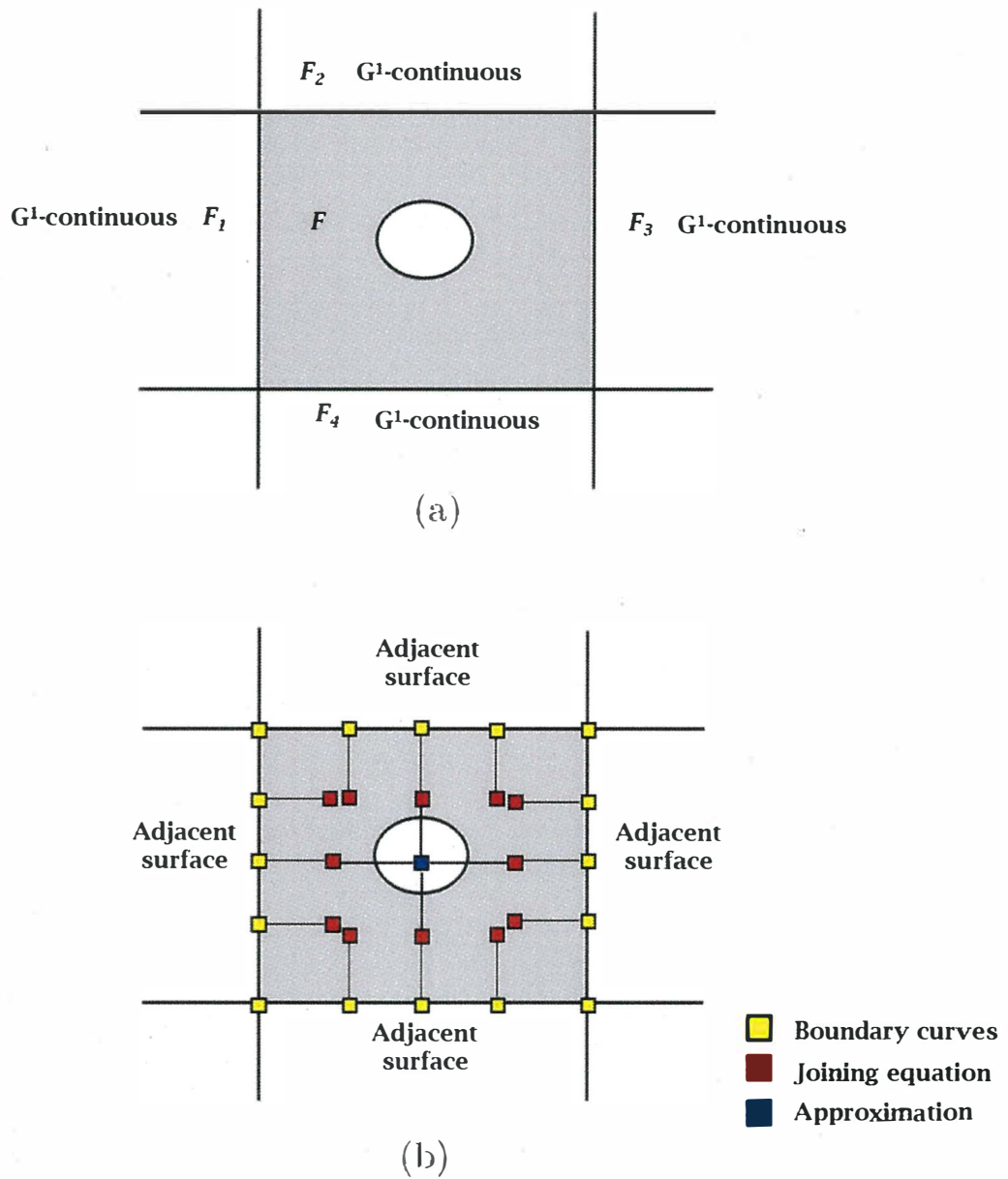


Figure 3.1: Concept of our proposed method (b) applied to the gray region of (a).

3.4 Joining With the Adjacent Surface

In this section an algorithm is described to connect two surfaces with G^1 -continuity. In this method, cubic Bézier curves are used for input boundary curve meshes. In order for two surfaces \mathbf{S}^1 and \mathbf{S}^2 , with a common boundary curve shown in Figure 3.2(a) to have a G^1 -continuity, the derivative vectors on the boundary curves should satisfy the condition defined by Equation (3.7) [14], where $k(v)$ and $h(v)$ are scalar functions of v as shown in Equation (3.8) [14]. If the vectors are set to $\mathbf{a}_i (i = 0, \dots, 3)$, $\mathbf{b}_i (i = 0, \dots, 3)$, $\mathbf{c}_i (i = 0, \dots, 2)$ as shown in Figure 3.2(b). The G^1 -continuous control points are calculated by solving Equation (3.9) and Equation (3.10) (see APPENDIX A for the derivation), where k_0, k_1 are positive real numbers and h_0, h_1 are arbitrary real numbers. To be more concrete, the cross boundary derivatives of the two surfaces are calculated by the joining equations [14], and control points which G^1 -continuous with adjacent surfaces are obtained. The obtained cross boundary derivatives serve as a condition for connecting two surfaces with G^1 -continuity.

$$\frac{\partial \mathbf{S}^2(0, v)}{\partial u} = k(v) \frac{\partial \mathbf{S}^1(1, v)}{\partial u} + h(v) \frac{\partial \mathbf{S}^1(1, v)}{\partial v} \quad (3.7)$$

$$\begin{aligned} k(v) &= k_0(1 - v) + k_1v \\ h(v) &= h_0(1 - v) + h_1v \end{aligned} \quad (3.8)$$

$$\begin{aligned} \mathbf{a}_0^3 &= \frac{\mathbf{a}_0 + \mathbf{b}_0}{|\mathbf{a}_0 + \mathbf{b}_0|} \\ \mathbf{a}_1^3 &= \frac{2\mathbf{a}_0^3 + \mathbf{a}_3^3}{3} \\ \mathbf{a}_2^3 &= \frac{\mathbf{a}_0^3 + 2\mathbf{a}_3^3}{3} \\ \mathbf{a}_3^3 &= \frac{\mathbf{a}_3 + \mathbf{b}_3}{|\mathbf{a}_3 + \mathbf{b}_3|} \end{aligned} \quad (3.9)$$

$$\begin{aligned} \mathbf{b}_0 &= k_0\mathbf{a}_0 + h_0\mathbf{c}_0 \\ \mathbf{b}_3 &= k_1\mathbf{a}_3 + h_1\mathbf{c}_2 \\ \mathbf{b}_1 &= \frac{(k_1 - k_0)\mathbf{a}_0^3}{3} + k_0\mathbf{a}_1^3 + \frac{2h_0\mathbf{c}_1}{3} + \frac{h_1\mathbf{c}_0}{3} \\ \mathbf{b}_2 &= k_1\mathbf{a}_2^3 - \frac{(k_1 - k_0)\mathbf{a}_3^3}{3} + \frac{h_0\mathbf{c}_2}{3} + \frac{2h_1\mathbf{c}_1}{3} \end{aligned} \quad (3.10)$$

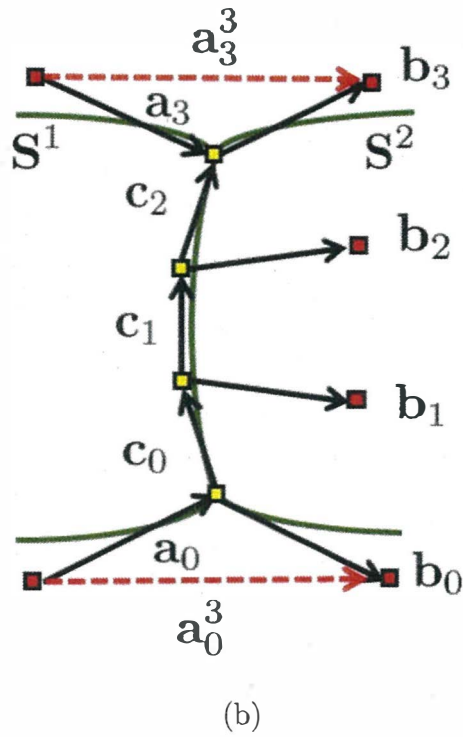
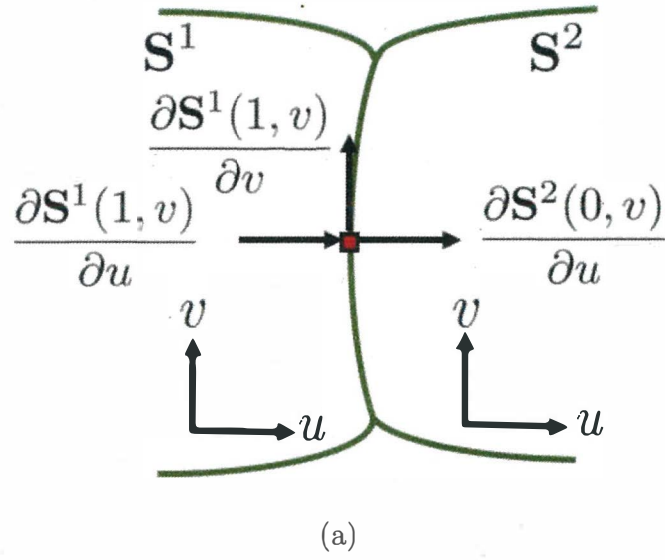


Figure 3.2: (a) G^1 -continuity condition and (b) connection of two surfaces using the joining equations [14].

3.5 Approximation

In this section, approximation of the inner control point of the generated surface is described. Firstly, the boundary information and sample points on the boundary edges which represent a hole are used to approximate the inner control point by the least squares approximation method. Next, a new surface is constructed using the Equation (3.1). Details of the approximation process will be described in section 3.5.1.

3.5.1 Approximation Process

Our approximation process is described in this section. In Figure 3.3, our approximation process of the inner control point is shown. As our concept of proposed method explains in section 3.3, knots are inserted at parameters $u_0 = 0.5$ and $v_0 = 0.5$ ($p = 0, q = 0$). The process is executed in the following steps:

1. The G^1 -continuous control points are obtained from joining equations and bi-cubic Gregory patch is constructed. The vectors between control points $\mathbf{b}_i, \tilde{\mathbf{b}}_i$ ($i = 0, \dots, 3$) are calculated for u direction. The vectors $\mathbf{d}_j, \tilde{\mathbf{d}}_j$ ($j = 0, \dots, 3$) are calculated for v direction.
2. Knots are inserted in both u and v directions. After knot insertion, vectors $\mathbf{r}_i = u_0 \mathbf{b}_i$ ($i = 0, \dots, 4$) are calculated and vectors $\tilde{\mathbf{r}}_i, \mathbf{v}_j, \tilde{\mathbf{v}}_j$ are calculated in the same manner. Moreover, control points are obtained from scaled vectors $\mathbf{r}_i, \tilde{\mathbf{r}}_j$ and $\mathbf{v}_j, \tilde{\mathbf{v}}_j$ as shown in Figure 3.3.
3. The points on the boundary edges which represent a hole are calculated as sample points and the center point of the hole is also added to the sample points. It is better to add center point to the sample points because it will improve the approximation accuracy around the hole. In our method, each boundary edge which represent a hole is equally divided into 10 sections, because in the range of this experiment, 10 sections was enough for the least squares approximation. The number of sample points $t = \text{the number of boundary edges which represent a hole} \times 10 + 1$ are assumed to be \mathbf{Q}_s ($0 \leq s \leq t$). The parameters of \mathbf{Q}_s are assumed to be (\bar{u}_s, \bar{v}_s) , and they are calculated by projecting \mathbf{Q}_s onto the Gregory patch constructed in step 1.

4. From the control points generated in step 2 and the sample points generated in step 3, the unknown inner control point is approximated by using Equation (3.11) (see APPENDIX B for the details of approximation method).
5. A new surface is constructed by the control points which were obtained in step 2 and the approximated inner control point which was obtained in step 4.

$$f = \sum_{s=0}^t |Q_s - S(\bar{u}_s, \bar{v}_s)|^2 \quad (3.11)$$

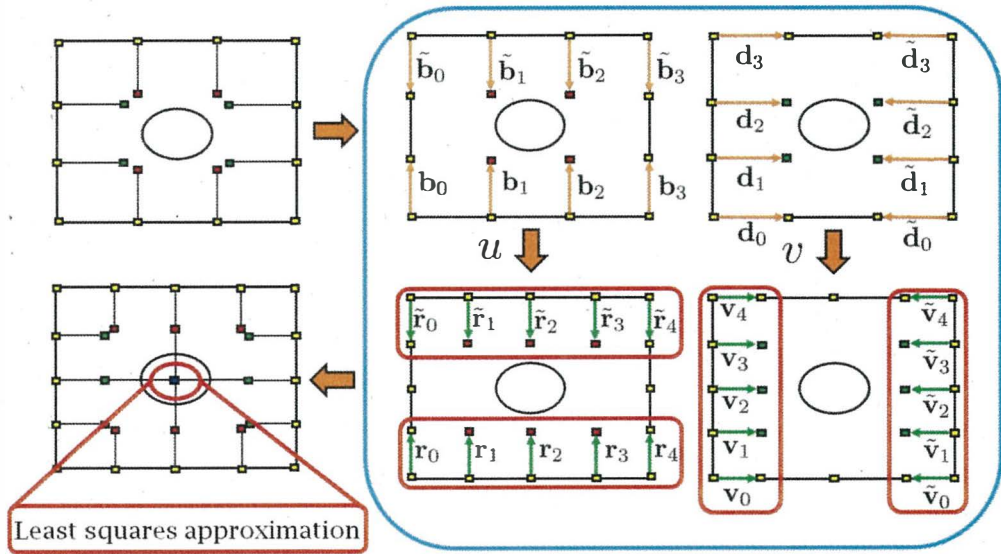


Figure 3.3: Inner control point approximation process.

3.6 Evaluation of Generated Surface

This section describes the evaluation method of the generated new surface. Our method was applied to the closed region with a hole obtained from CAD as shown in Figure 3.4 and the practicality was verified. To verify the accuracy of the generated surface, the distance between the generated surface and the source surface retained by the trimmed surface is measured. The source surface was divided equally in both u and v directions into twenty sections so that a square grid was generated. The generated grid points on the source surface are projected to the generated surface and the distance between the source surface and generated surface is measured. Moreover, to find a relative error, the ratio of the bounding box size and the maximum distance are calculated [7]. In this thesis, when ratio is smaller than 1% [7, 25], it is assumed that a shape is approximated in good accuracy as a reference model for downstream processes.

3.7 Experimental Results

Our method is applied to the shapes with a hole obtained from CAD data and the practicality was verified as shown in Figures 3.5 to 3.8. The generated surfaces were evaluated with the evaluation method described in section 3.6. Figure 3.5(a) shows the control points of generated surface F that has G^1 -continuous adjacent surfaces F_1 and F_2 in two directions. Figures 3.5(b), 3.6(a), 3.6(b) and 3.7(a) shows the control points of generated surface F that has G^1 -continuous adjacent surfaces F_1 , F_2 and F_3 in three directions. Figures 3.7(b) and 3.8 shows the control points of generated surface F that has G^1 -continuous adjacent surfaces F_1 , F_2 , F_3 and F_4 in all directions. The red dots indicate the control points generated in step 2 and the blue ones indicate the approximated control point in step 4, described in section 3.5.1.

In Table 3.1, data from A to G represent the practical CAD data used in our experiment. The error evaluation of the generated surface is shown in Table 3.1, *Avg.* indicates the average error margin value obtained by averaging the distances between the generated surface and the source one. *Max* indicates the maximum error margin value representing the maximum distance between the generated surface and the source one. *Ratio*(%) indicates

the ratio of the bounding box size and the maximum distance. The ratio of all objects from A to G are less than 1% as shown in Table 3.1, and we can find that shapes are approximated in good accuracy as reference models for downstream processes. As described as the step 3 in the section 3.5.1, it is better to add the center point to the sample points because it will improve the approximation accuracy around the hole. Table 3.2 shows the difference of error margins around the hole, obtained by adding the center point to the sample points. We can find that the approximation accuracy improved both on the average and maximum error margin values around the hole area by adding center point to the sample points. Additionally, the discrete evaluation result of a surface overall shape was visualized by generating a color map within a range of the distances between the generated surface and the source surface as shown in Figures 3.9 and 3.10. The blue indicates the minimum error margins and the red indicates the maximum error margins on the surface in Figures 3.9(a), 3.9(b), 3.10(a) and 3.10(b). We can also see the improvement of the approximation accuracy around the hole area by adding the center point to the sample points, from the enlarged views as shown Figures 3.9 and 3.10. Because of the original data inconsistency of shape E, the maximum error margin value is bigger than the other experimental data as shown in the Table 3.1 and as well as in the Figure 3.10(b).

Furthermore, in order to verify the continuity with adjacent surfaces, the normal vectors on the boundary edges of the generated surface are calculated, shown with blue lines in Figures 3.11 to 3.14 and those of the adjacent surfaces are shown with red lines. As shown in Figures 3.11 to 3.14 the normal vectors of the generated surfaces coincide with those of the adjacent surfaces on their boundary edges, and we can find that two surfaces are connected with G^1 -continuity.

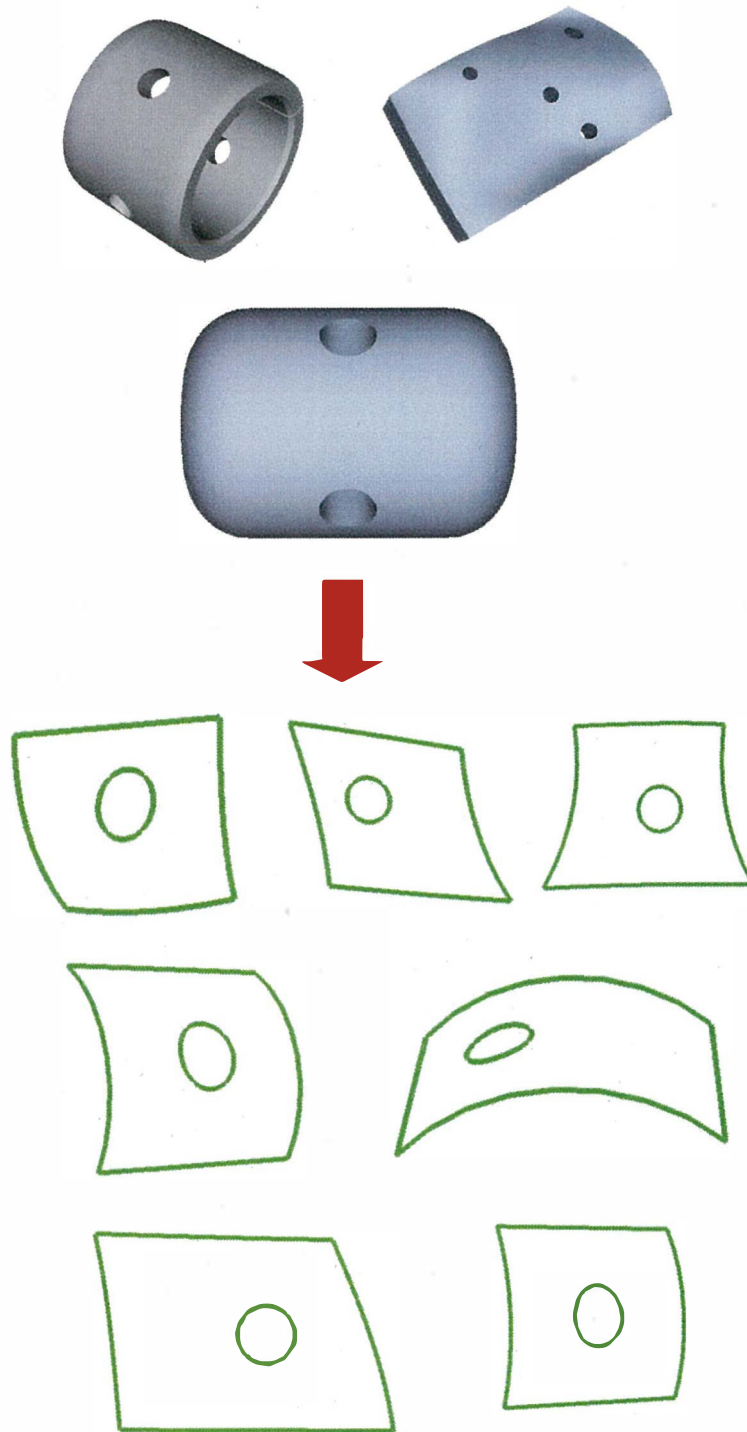
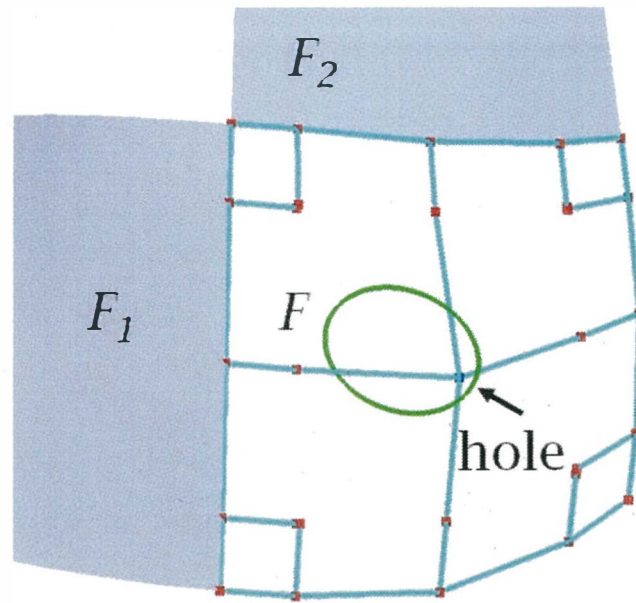
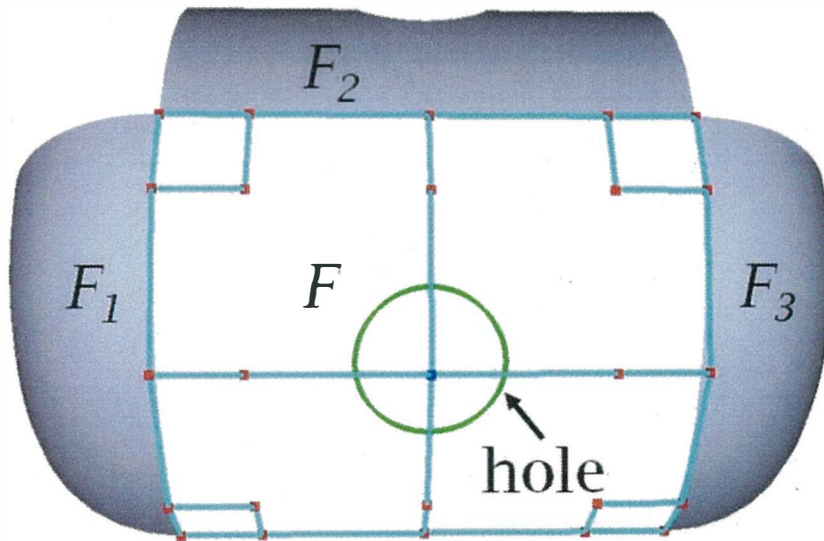


Figure 3.4: Closed region obtained from CAD.

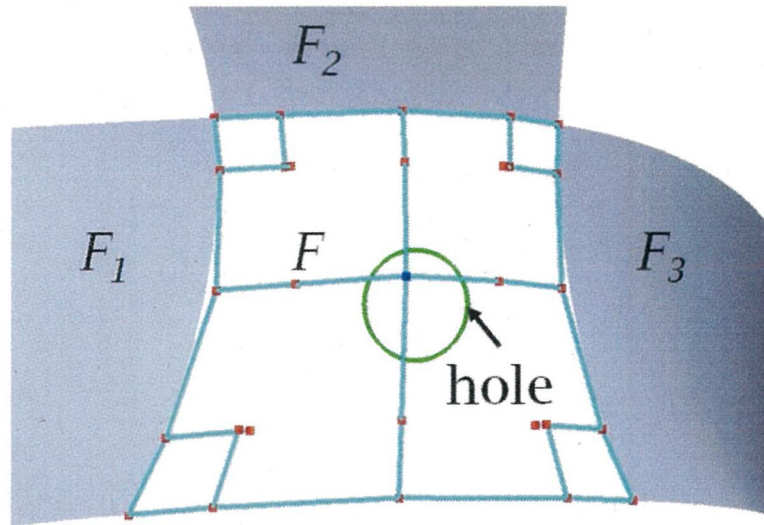


(a)

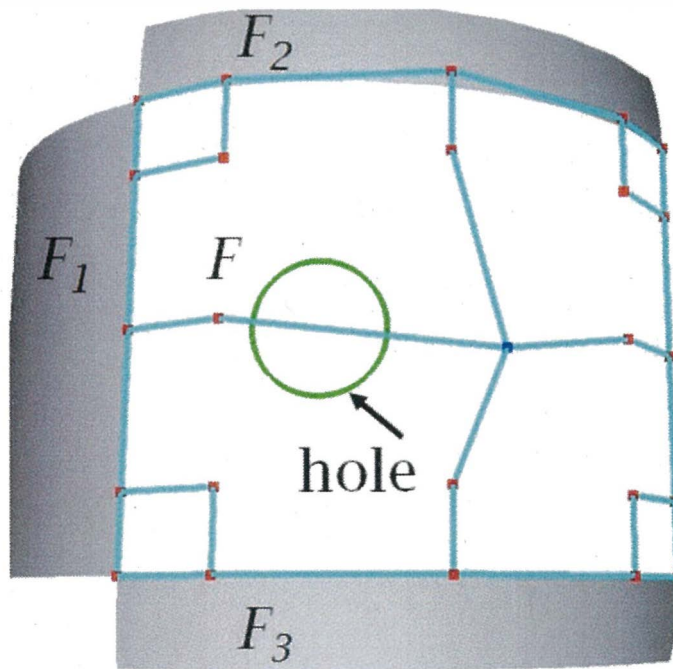


(b)

Figure 3.5: (a) control points of generated surface A, (b) control points of generated surface B.

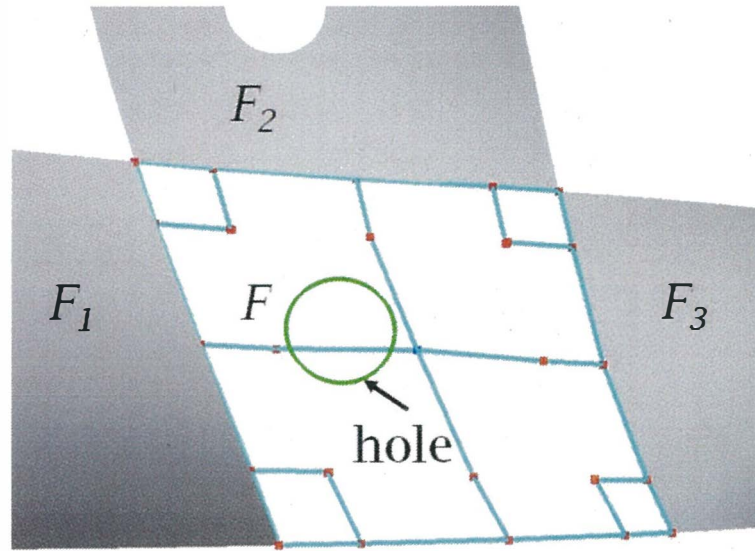


(a)

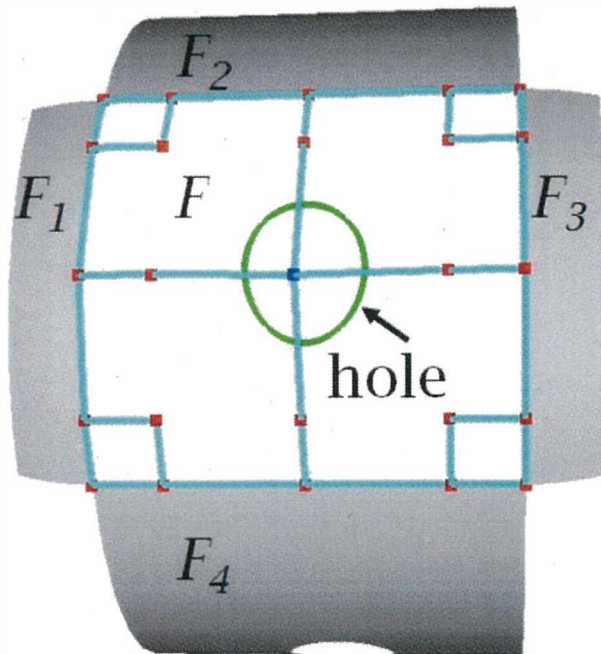


(b)

Figure 3.6: (a) control points of generated surface C, (b) control points of generated surface D.



(a)



(b)

Figure 3.7: (a) control points of generated surface E, (b) control points of generated surface F.

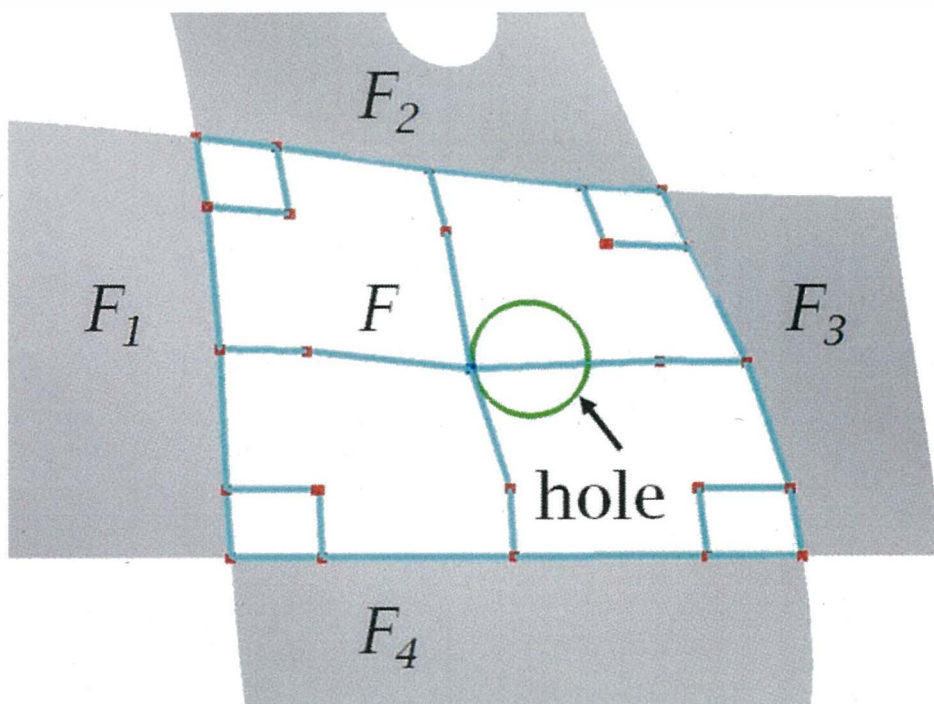


Figure 3.8: Control points of generated surface G .

Table 3.1: Error evaluation of the source surface and the generated surface.

<i>Object</i>	<i>Evaluationobject</i>	<i>Avg.</i>	<i>Max</i>	<i>Ratio(%)</i>
A	Trimmed surface	0.582885	1.865794	0.388339
B	Trimmed surface	0.005640	0.024776	0.049194
C	Trimmed surface	0.352679	1.139214	0.253059
D	Trimmed surface	0.012622	0.068239	0.460547
E	Trimmed surface	1.205581	4.220689	0.817447
F	Trimmed surface	0.002428	0.011756	0.092034
G	Trimmed surface	0.225614	0.895673	0.182698

Table 3.2: Difference of error margins around the holes obtained by adding the center point to the sample points.

<i>Data</i>	<i>With center point(Y)</i>		<i>Without center point(N)</i>		<i>Difference(Y - N)</i>	
	<i>Avg.</i>	<i>Max</i>	<i>Avg.</i>	<i>Max</i>	<i>Avg.</i>	<i>Max</i>
A	0.969301	1.578882	0.967025	1.589873	0.002276	-0.010991
B	0.026929	0.029018	0.063070	0.066205	-0.036141	-0.037187
C	0.284248	0.601748	0.303415	0.741213	-0.019167	-0.139465
D	0.009415	0.017530	0.009912	0.022806	-0.000497	-0.005276
E	0.706996	1.228102	0.750653	1.287324	-0.043657	-0.059222
F	0.010209	0.012188	0.011112	0.013014	-0.000903	-0.000826
G	0.243074	0.543374	0.248200	0.557874	-0.005126	-0.014500

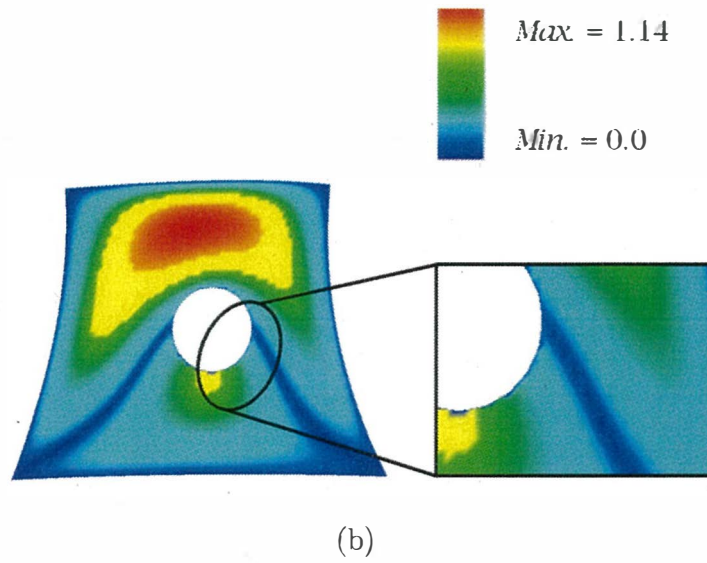
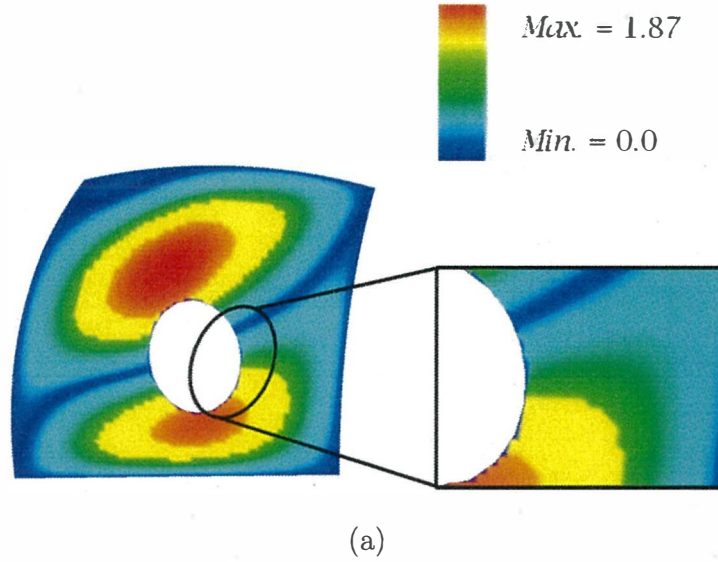
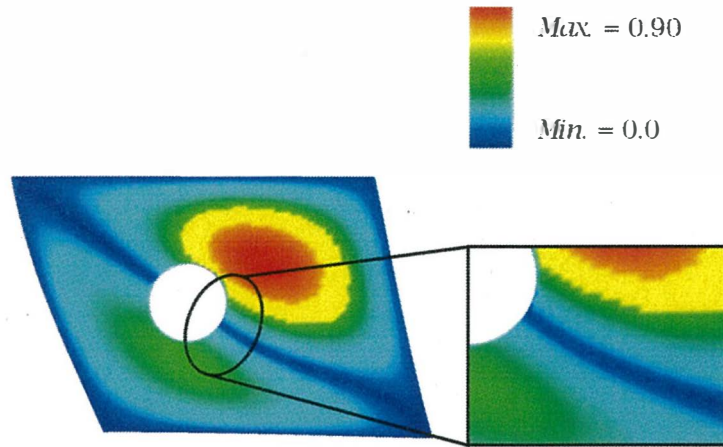
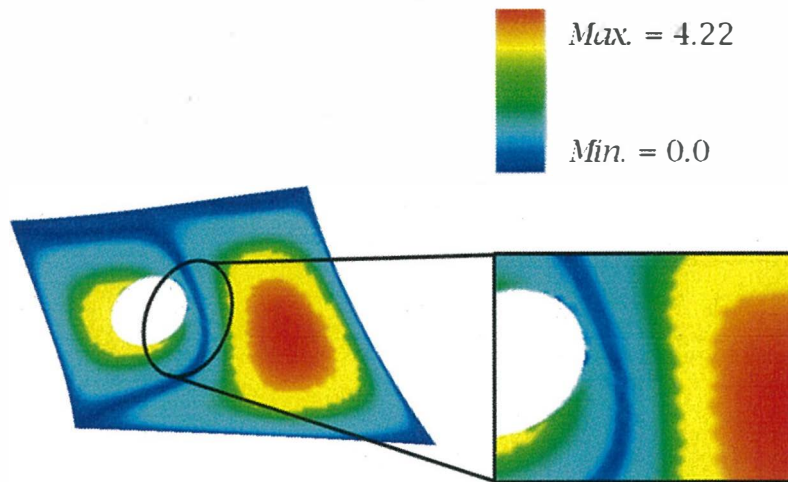


Figure 3.9: Result of surface evaluation: distances between the generated surface and the source one are calculated. (a) and (b) are the error margins of objects A and C respectively in the Table 3.1.

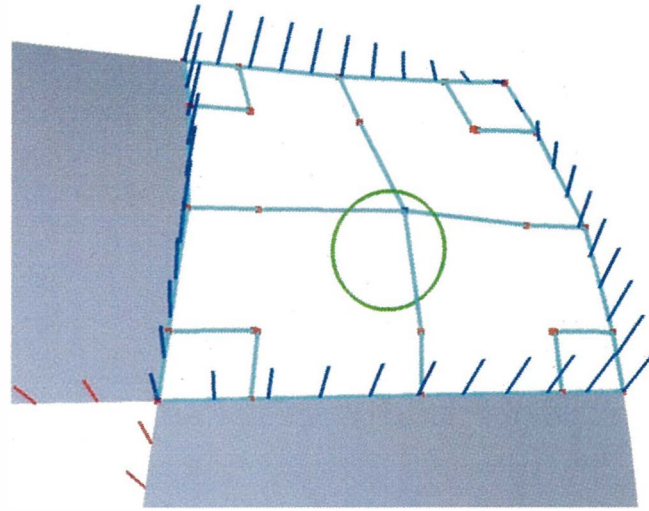


(a)

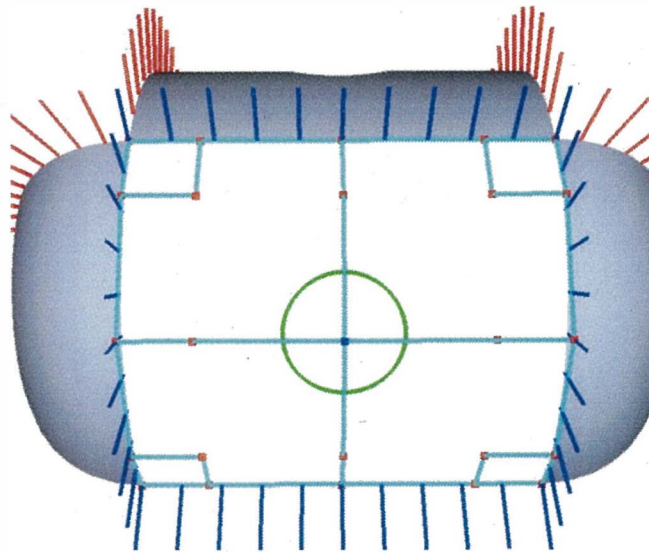


(b)

Figure 3.10: Result of surface evaluation: distances between the generated surface and the source one are calculated. (a) and (b) are the error margins of objects E and G respectively in the Table 3.1.

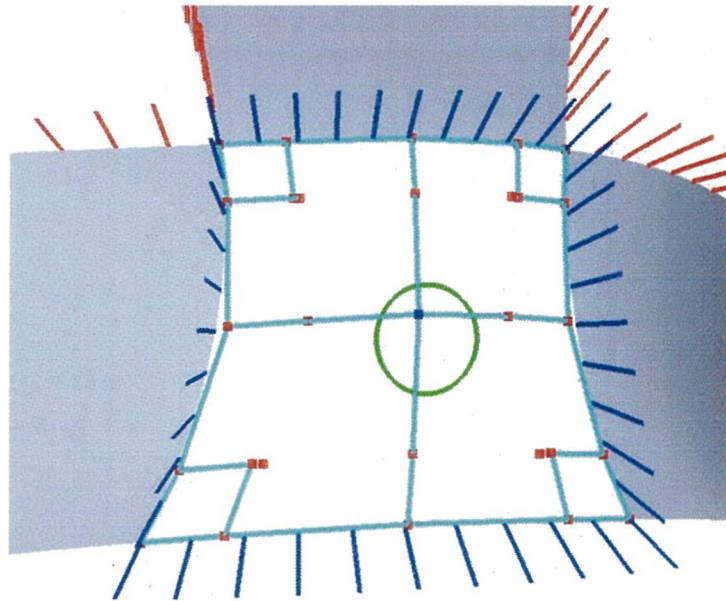


(a)

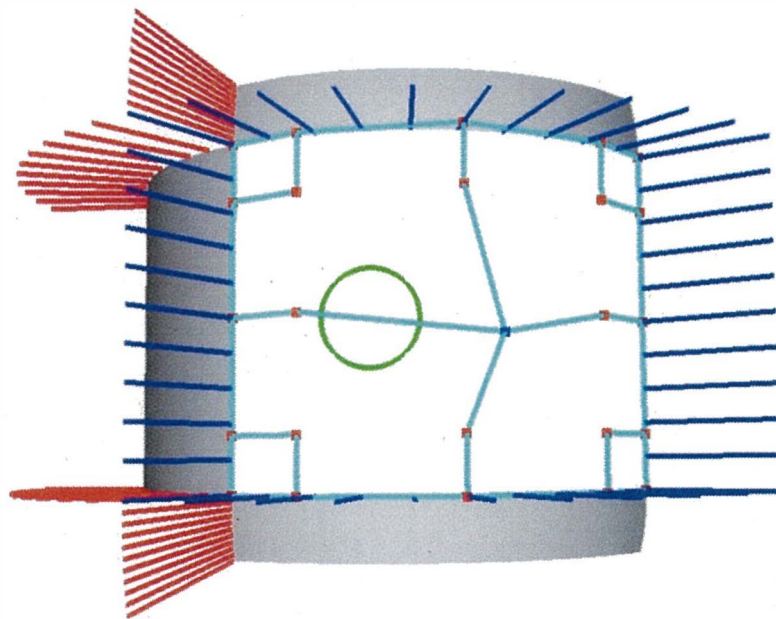


(b)

Figure 3.11: Verification of the continuity with adjacent surfaces: the normal vectors of the generated surfaces A and B are coincide with those of the adjacent surfaces on their boundary edges.

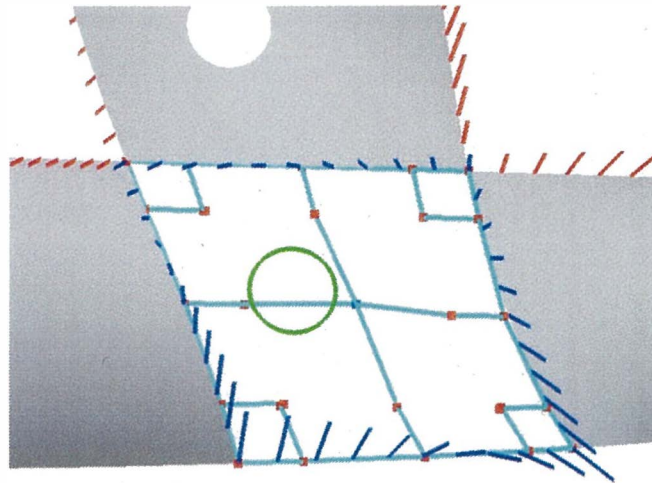


(a)

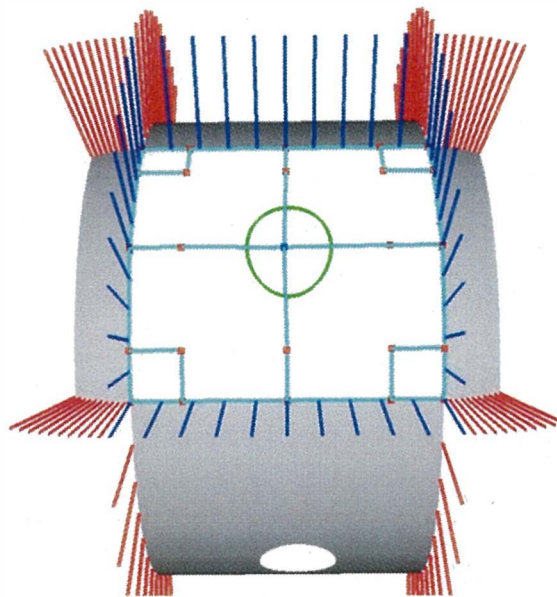


(b)

Figure 3.12: Verification of the continuity with adjacent surfaces: the normal vectors of the generated surfaces C and D are coincide with those of the adjacent surfaces on their boundary edges.



(a)



(b)

Figure 3.13: Verification of the continuity with adjacent surfaces: the normal vectors of the generated surfaces E and F are coincide with those of the adjacent surfaces on their boundary edges.

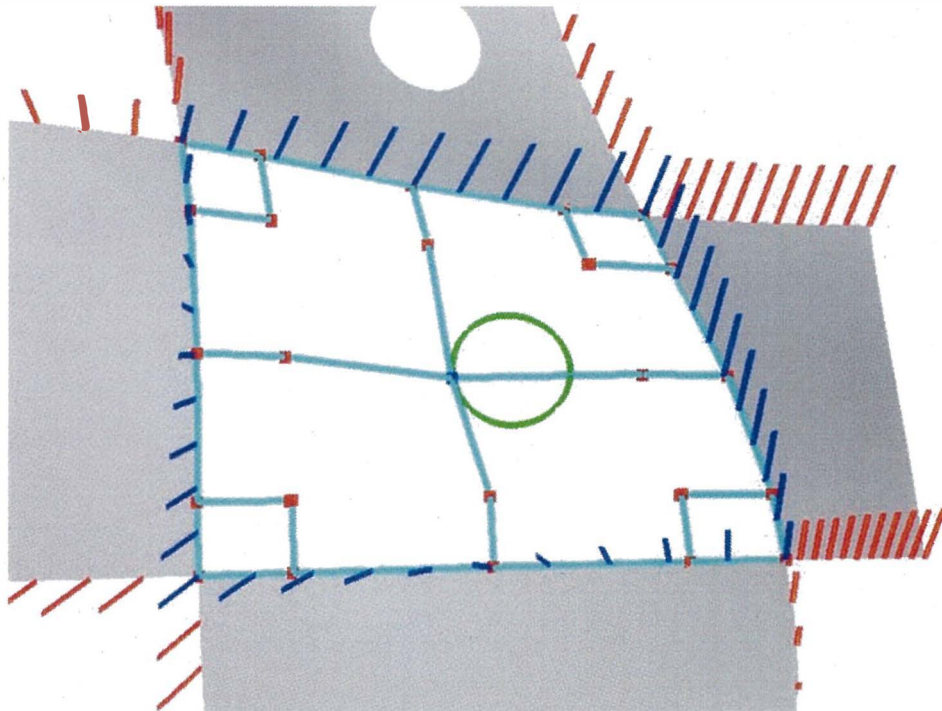


Figure 3.14: Verification of the continuity with adjacent surfaces: the normal vectors of the generated surface G coincide with those of the adjacent surfaces on their boundary edges.

3.8 Summary

In this thesis, we have proposed the method of generating a smooth surface with a hole that connects to adjacent surfaces with G^1 -continuity by applying our new surface representation to a closed region. The proposed method integrates the advantages of the Gregory and B-spline surfaces. Concretely, the inner control points are obtained based on least squares approximation method, and the G^1 -continuous control points on the boundary are obtained from the joining equations as described in section 3.5. Moreover, our method is independent of the position and the hole shape. Our method is also applicable to a region surrounded by surfaces in all directions connecting with G^1 -continuity. Since our method generates a surface from boundary edge information, it is applicable to various applications. For instance, by including our method in the trimmed surface compression method [6, 25], a smooth surface with good quality can be generated. It is also effective for direct modeling where shapes with a hole are modified.

In our method, by integrating the Gregory and B-spline surfaces, a smooth surface is generated in good accuracy for a downstream process as a reference model. Therefore, it is necessary to implement the new surface representation. In this thesis, on a common boundary where two surfaces are connected with G^1 -continuity, an input curve mesh is represented by cubic Bézier curves and the G^1 -continuous control points on the boundary are obtained from the joining equations. Therefore, it is necessary to extend our method so that it can be applied to shapes with complex composite boundary curves or B-spline curves with multiple segments.

Chapter 4

3D Data Compression and Retrieval Application

4.1 Introduction

In this chapter, the contribution to the development of the current 3D data compression and retrieval method is described first. Then, evaluation of the 3D data compression and retrieval application system is described. Moreover, the performance of 3D data compression and retrieval application system is evaluated with different network environments: such as third generation of mobile telecommunications (3G) and Worldwide Interoperability for Microwave Access (WiMAX). As the result, we confirmed the effectiveness of the compression method with practical data.

4.2 Background

Digital mock-up (DMU) and/or compound document with 3D data are one of the most important methods to represent a product model. Since the data size of 3D models becomes greater year by year, and the gigantic data size is one of the biggest obstacles with the communication between downstream applications using the 3D data designed with 3D CAD systems. As a result, 3D data compression and retrieval algorithm is required to easily exchange

such information through the Internet. Because broadband is still not popular in some regions in the world, it is necessary to send huge data in a small size as much as possible. Therefore, in this thesis the development of an application system that transfers 3D surface models are explained and then the performance of the 3D surface compression and retrieval algorithm is evaluated.

Manufacturing has been globalized during the last two decades. Designed and manufactured by the manufacturing facilities around the world have been routinely performed. From a manufacturer's perspective, 3D data is beneficial information because it allows visualization of exactly what the finished product being made will look like. This can be particularly helpful when dealing with complex geometries that difficult to interpret from a 2D drawing alone. Therefore, a mechanism that distributes the 3D data, designed in design division, to the world is required. Because broadband is still not popular in some regions in the world, 3D data compression and retrieval method is an important issue for reducing the latency of 3D data transmission with Internet access.

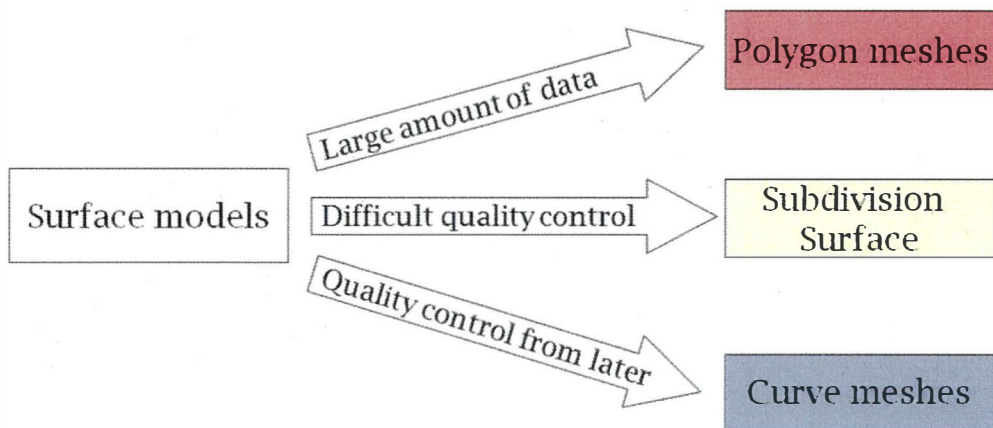
A number of methods have been developed to compress 3D surface models in the past few years; As shown in Figure 4.1, there are 3 surface model representations that used in compression of 3D data models:

- Based on polygon meshes.
- Based on subdivision surface.
- Based on curve meshes.

The amount of data will become large in polygon meshes. Since the division number becomes n -th power of 2, it is difficult to control quality with subdivision surface. In contrast, On curve meshes representation the quality can be controlled later on and the precision controllable surface model can be generated. Therefore, it is a best candidate for compression of surface models. In addition, Wakita et al. [24] adopted surface interpolation method using Gregory patches [26]. However, the surface interpolation method cannot be applied to the concave shapes or shapes with holes as described in section 2.1. To overcome this problem, Muraki et al. proposed a surface compression

method using a surface fitting method [6, 7]. In his paper, the data compression technique of 3D model is mentioned. However, any retrieval method is not evaluated and compressed file transfer is not performed.

In this thesis, the performance of the 3D surface compression and retrieval algorithm based on a curve mesh interpolation [26] and N-side filling [6, 7] is evaluated. To be more concrete, an application system that transfers 3D surface models has been firstly developed. After that, the performance is evaluated with different network environments: such as third generation of mobile telecommunications (3G) and Worldwide Interoperability for Microwave Access (WiMAX). As the result, we confirmed the effectiveness of our compression method with practical data.



The precision controllable surface model can be generated

Figure.4.1: Data compression of 3D data models.

4.3 Surface Compression Method

4.3.1 Concept of Surface Compression Method

In this section, the main concept of surface compression method is described. Surface compression method is composed of “**Compression part**” and “**Retrieval part**”. Figure 4.2 illustrates the main concept of our data com-

pression and retrieval method. In data compression part, surface elements are alternatively removed from 3D shape data to reduce the data size. When surface elements are deleted, the prediction function for the deleted surface is saved as attribute information. First, surface interpolation method and N-side filling method are applied to a closed region. After that, errors are evaluated for the generated surface. When it is judged that the surface can be fitted with good accuracy, the corresponding surface element will be removed. Here, based on surface fitting method what can be removed determines the compression ratio of the data size. In retrieval part, the received data is used to retrieve the surface data. A surface is fitted by using boundary edges and the prediction function of the attribute information, and the 3D shape model will be reconstructed.

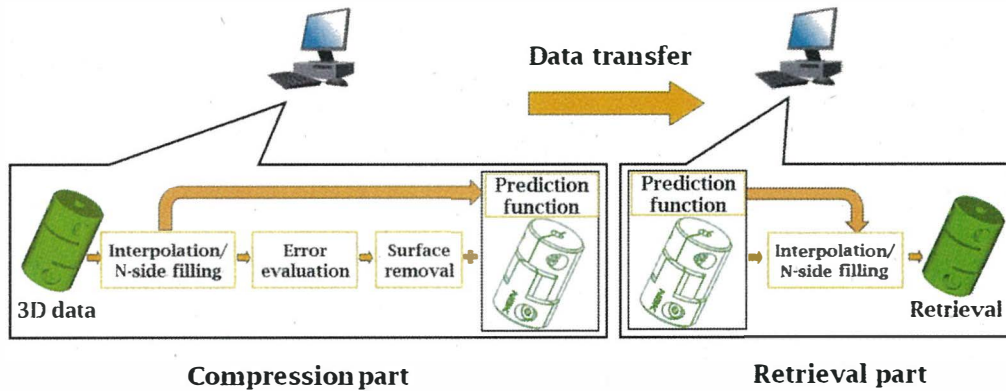


Figure 4.2: Concept of 3D data compression and retrieval method.

4.3.2 Compression Part

In our method, the 3D data is compressed by estimating a surface that approximates from a boundary curve mesh, and then the original surface is deleted if the approximated surface is suitable. The compressed data can be retrieved from the boundary curve mesh in the same manner as the approximation of the compression process. To compress data easily, 3D surface type is classified into four elements; 1) Plane, 2) Interpolated surface, 3) Surface fitted with the N-side filling method, and 4) other surface. Elements 1) to 3) are

generated from the boundary edges by using our approach. Element 4) represents the complex trimmed surface that is difficult to apply to the method described in section 2.3. The surface element is removed when the surface can be approximated within the tolerance. As the base surface of trimmed surface, contained in shape models, can be removed with this technique, it is possible to express the shape models with curve mesh representation. As a result, the amount of data is greatly reduced. The information of the method, the surface interpolation method or N-side filling method that should be applied to the four surface types, is indicated with the prediction function. The prediction function for the removed surface is added to the face as attribute information. The 3D shape model can be retrieved from the boundary curves with the prediction function.

Both interpolation method and N-side filling method are difficult to apply to composite surfaces. It is difficult to fit a composite surface even in the case of the simple shapes whose boundary curves are closed to quadrilateral region. This is because the base surface has a large rough area or twisted boundary curves. Therefore, a composite surface must be appropriately divided after surfaces are generated and evaluated with the tolerance. If this operation is acceptable, the original surface elements are removed. In our method, the surface element removal must be performed in the last stage of processing because the continuity of surfaces may collapse if it is performed in order. The compression stage of our method costs the calculation because the iterative calculations are required. For reducing the computational cost in the retrieval stage, some precalculated information is stored in the prediction function.

4.3.3 Flow Chart of Data Compression Part

Figure 4.3 shows the flow of compression process. The flow of the process is described as below:

1. Import all the surfaces to be compressed.
2. Judge for surface type 1) plane. By applying surface interpolation method or N-side filling method to the surface types 2) and 3), evaluate whether each surface is compressible or not. 3-sided region is judged whether can be interpolated with degenerated four-sided region and added to the surface type 2).

3. Save the value of the prediction function as the face attribute. The value of 1), 2) and 3) are set up as prediction function. Moreover, save some precalculated information along with the prediction function for reducing the computational cost in the retrieval stage. Details of this process is described in section 4.4.
4. Steps 2 and 3 are performed to all the surfaces.
5. According to the face attributes of 1) to 3), remove the surface data, and this step is performed to all the surfaces.
6. Output all the surfaces imported in step 1.

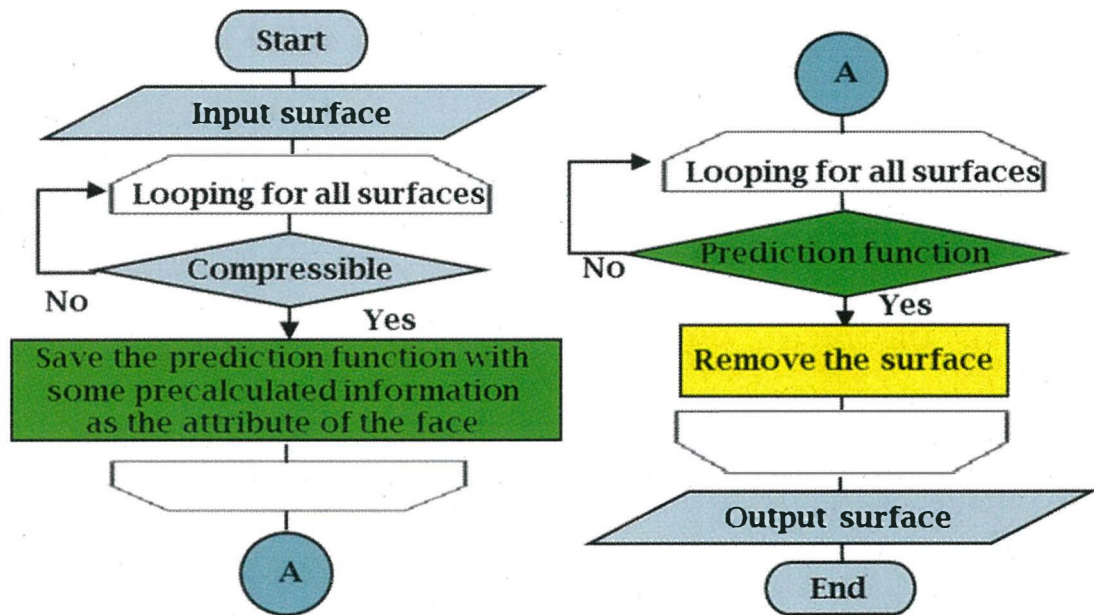


Figure 4.3: Flow chart of our compression process.

4.4 Surface Retrieval Method

4.4.1 Retrieval Part

In data retrieval part, the 3D surface model is retrieved from the boundary curves and the prediction function that is stored in the compression stage. To be more concrete, surface elements are retrieved from received boundary edges and prediction functions as shown in Figure 4.4. In Figure 4.4, according to prediction functions 1, 2 and 3 which method should be applied to the closed region is decided as follow:

- 1: holds the information for the surface interpolation method.
- 2: holds the information for the N-side filling method.
- 3: holds the information for accelerating the retrieval process.

In the compression stage, the error evaluation process is performed iteratively to make sure of the sufficiency of the generated surfaces. It is time consuming when the composite surface with the large number of control points is approximated, and the computational cost will be expensive. For avoiding these costs in the retrieval stage, it is necessary to add some practical information to the prediction function as attributes for generating surfaces. If the data size is reduced, the transmission time will be fast, but the retrieval cost will be high. For enhancing the time for retrieval, the precalculated information is used. To be more concrete, if the number of control points on approximated surfaces is more than a magical number N in the surface approximation process, the information that retrieves the surface are saved as the attributes. Processing for surface control point calculation by the N-side filling method is heavy. By adding such information to the attributes. the amount of computation can be reduced significantly. As the result, calculation cost of the surface generation can be reduced in the retrieval stage. Since the data size and calculation cost for retrieving surfaces are antinomy in each other, it is necessary to consider the balance of the data size and retrieval time by determining the added attributes with the number of surface control points. In our evaluation, in consideration of the balance between data size

and retrieval time, the magical number N , which is stored as the attributes, is set to 20.

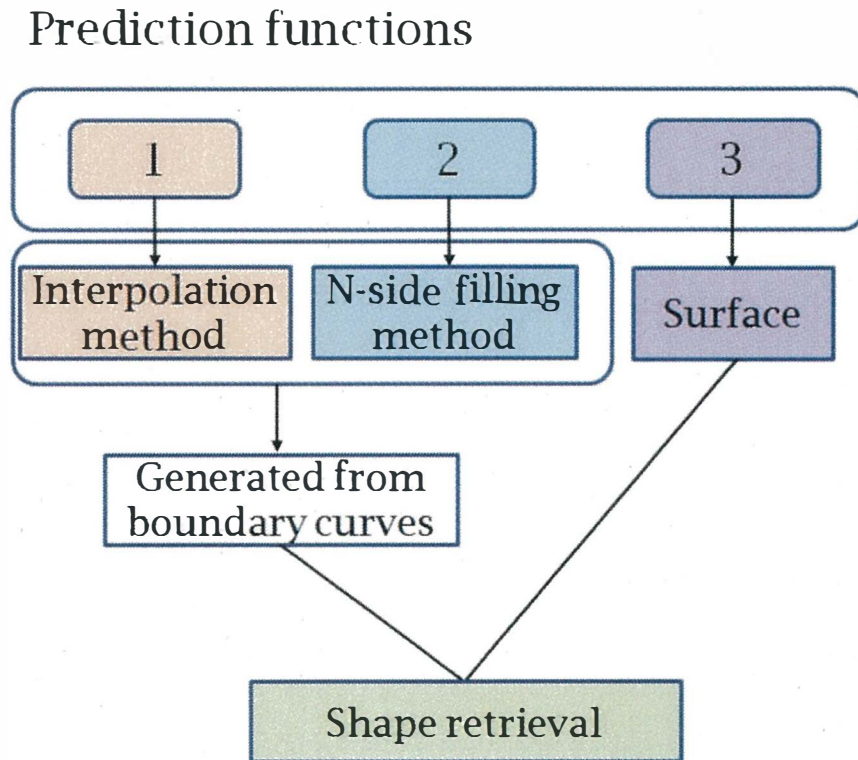
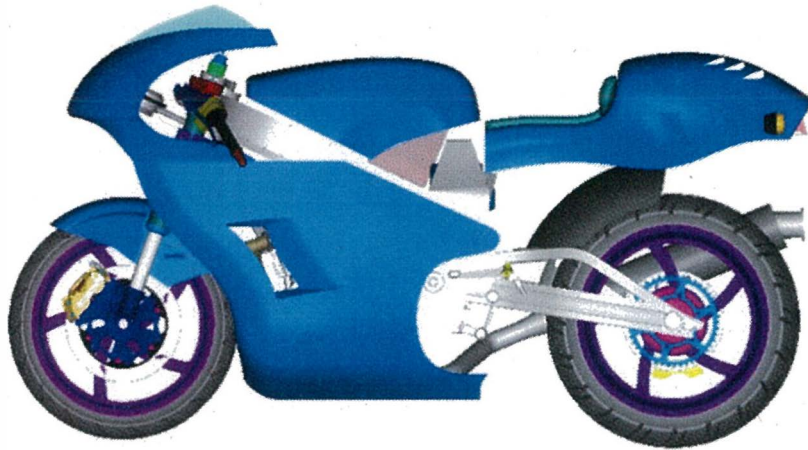


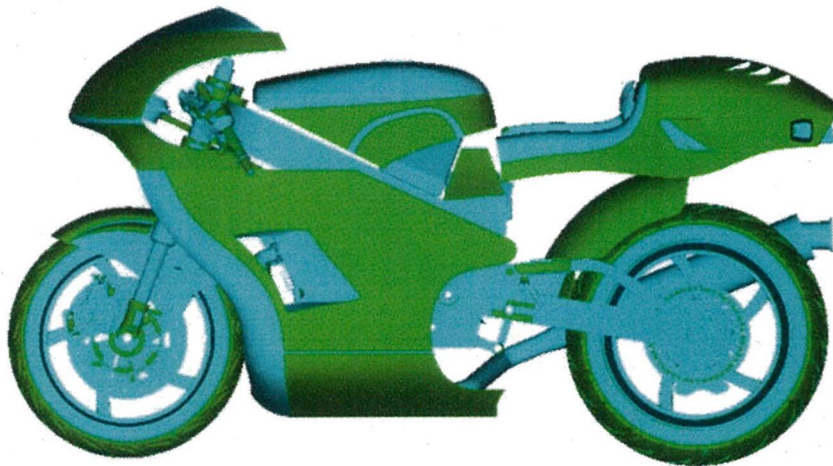
Figure 4.4: Flow chart of data retrieval process.

For example, Figure 4.5 shows the retrieval of compressed data by using surface fitting method [25]. Figure 4.5(a) represents the original IGES data. In Figure 4.5(b), surfaces whose compression and retrieval are succeeded are shown in cyan and those for which compression is failed are shown in green. Figure 4.6 shows only succeeded surfaces of Figure 4.5(b).

Figures 4.7(a) to (c), 4.8(a) and 4.8(b) are the enlarged views of some surface in Figure 4.5. Figure 4.7(a) shows the control points of the fitted surfaces by using the N-side filling method described in section 2.2. Figure 4.7(b) shows interpolation for a 3-side region by using the method [25]. Figures 4.7(c), 4.8(a) and 4.8(b) show the fitted surfaces by using the surface fitting method described in section 2.3.



(a)



(b)

Figure 4.5: Example of surface fitting method application.

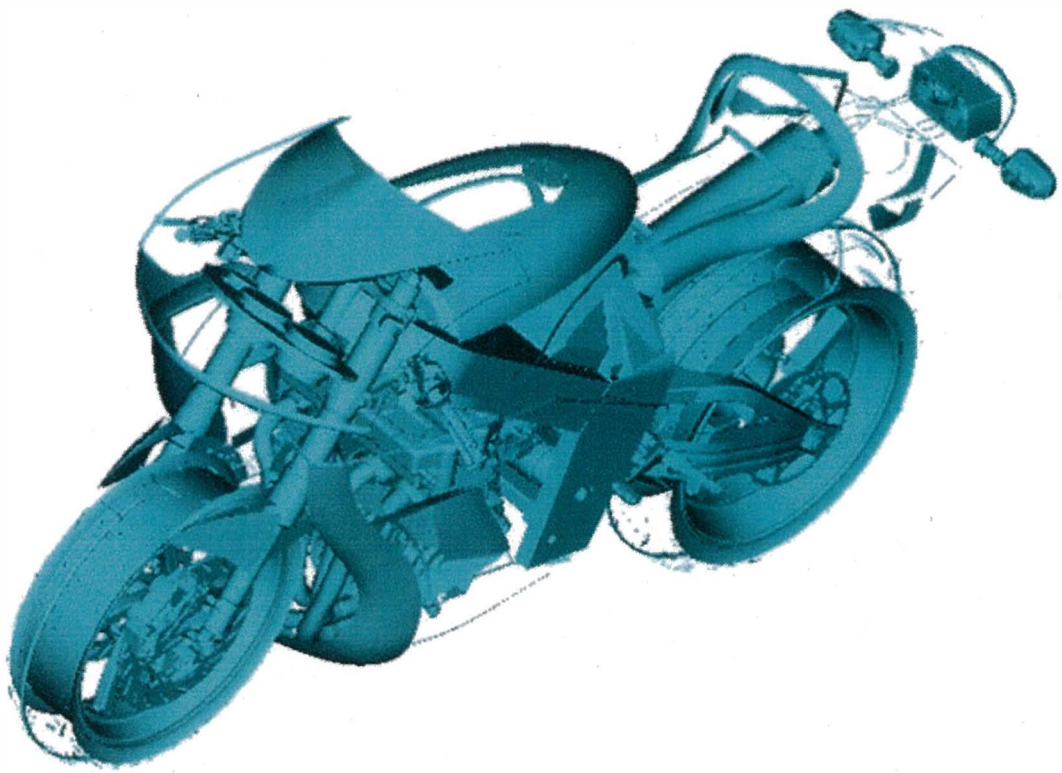
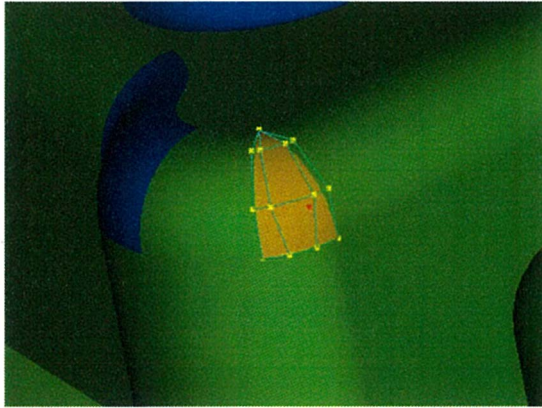


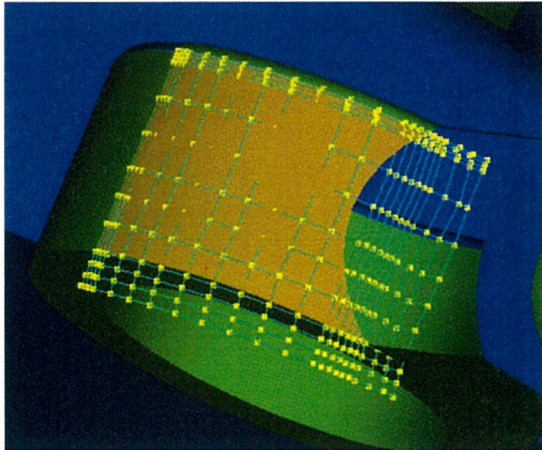
Figure 4.6: Example of surface fitting method application.



(a)

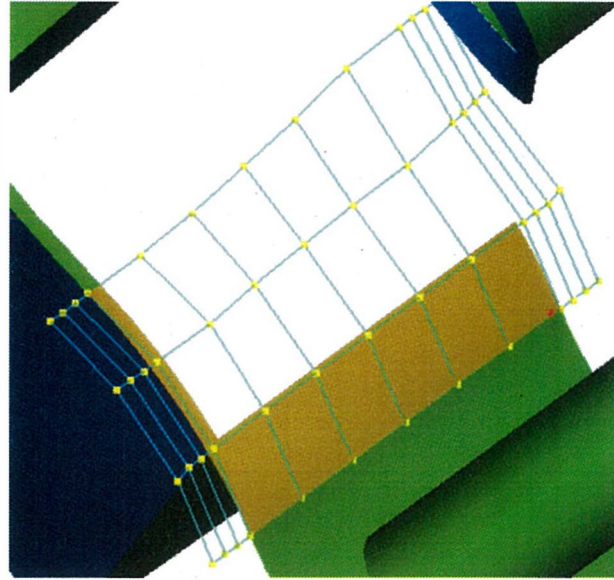


(b)

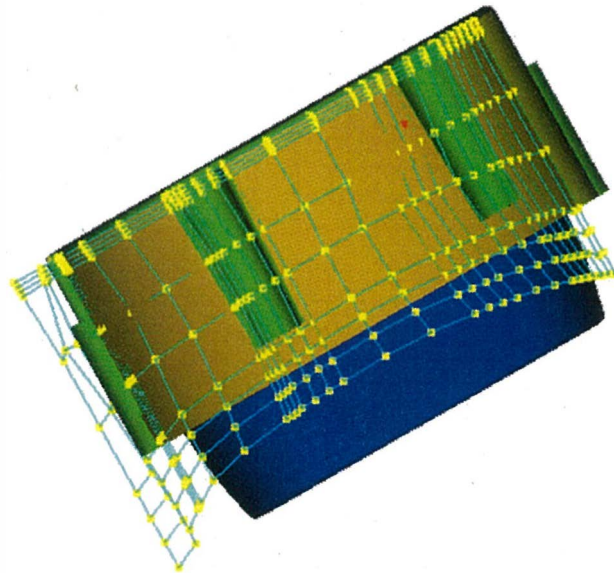


(c)

Figure 4.7: Details of surface fitting.



(a)



(b)

Figure 4.8: Details of surface fitting.

4.5 Experimental Results

In this section, the compression and retrieval method [25] is applied to CAD data in the IGES format, and practicality is verified. Three of the experiment IGES data and the result of the data retrieval are shown in Figures 4.9, 4.10 and 4.11. Figures 4.9(a), 4.10(a) and 4.11(a) represent the IGES data. Figures 4.9(b), 4.10(b) and 4.11(b) show the result of the data retrieval by using the method described in section 4.4. In Figures 4.9(b), 4.10(b) and 4.11(b), the surfaces for which data compression and retrieval are succeeded are shown in cyan. The method described in section 2.3 is difficult to apply to the complex trimmed surface. In our method, the surfaces for which compression is failed are shown in green. According to Figures 4.9(b), 4.10(b) and 4.11(b), we can find that the surfaces are generated in good accuracy as a reference model for the downstream processes.

4.6 Performance Evaluation Method

The evaluation is carried out in three phases. Figure 4.12 shows the flow of the evaluation.

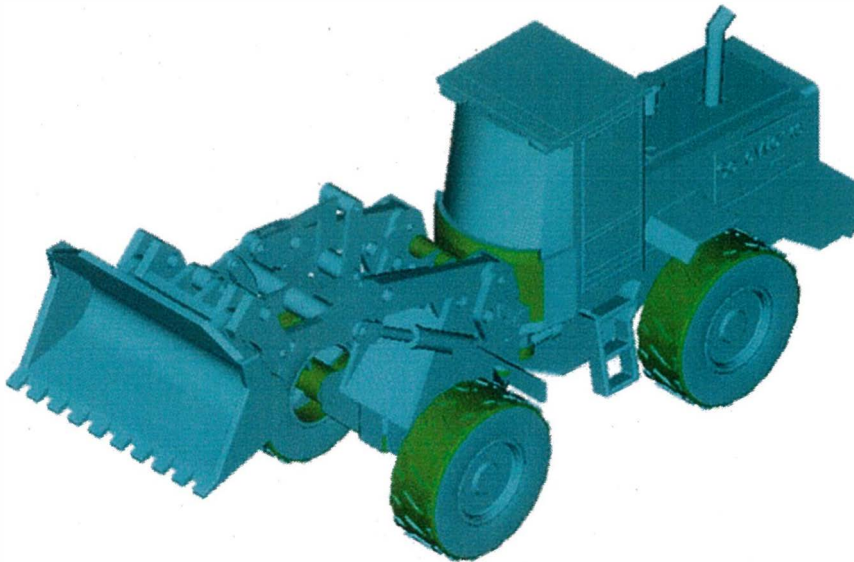
- First, for each of the same shape, prepare IGES data and the compression data based on this technique.
- Next, compare the file size of IGES data compressed in the Zip format and the data compressed using our compression method.
- Then, upload those data on the web server and measure the download time and the retrieval time of the downloaded data.

Two kinds of wireless devices, 3G and WiMAX, are used to measure the download time. Transmission speed of 3G is about 300Kbps in general and WiMAX is about 40Mbps. We define the time required for three processes, import (decompression) of the downloaded data, retrieval, and display of the data on a CAD viewer screen as “Retrieval time”.

Figure 4.13 shows experiment environments: such as PC information and download places. First, we downloaded the compressed files in 3 different



(a)



(b)

Figure 4.9: Example of surface fitting method application.



(a)

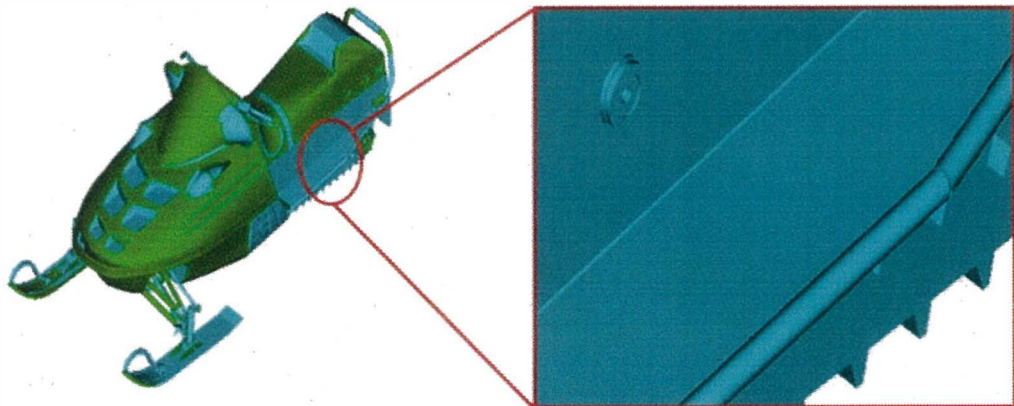


(b)

Figure 4.10: Example of surface fitting method application.



(a)



(b)

Figure 4.11: Example of surface fitting method application.

palaces with 3 different terminal speeds of network environment such as : station (3G), university (WiMAX1.0Mbps) and downtown (WiMAX1.5Mbps). And then, measured the retrieval time on Client PC.

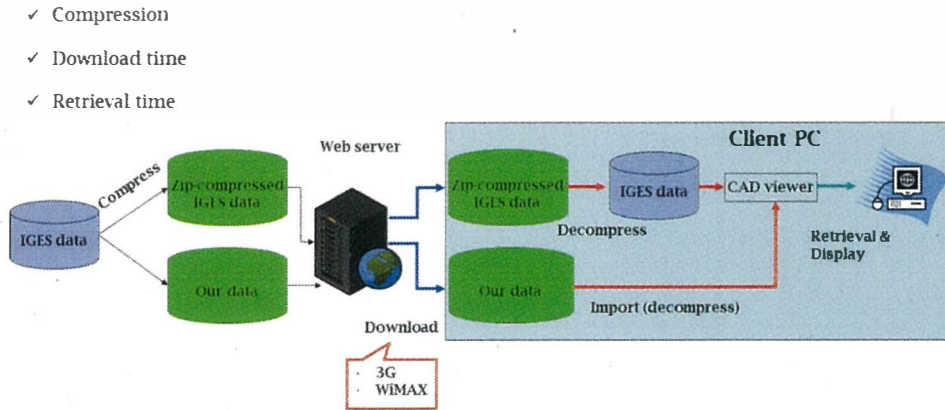


Figure 4.12: Evaluation flow for the total time required to display practical data on the screen.

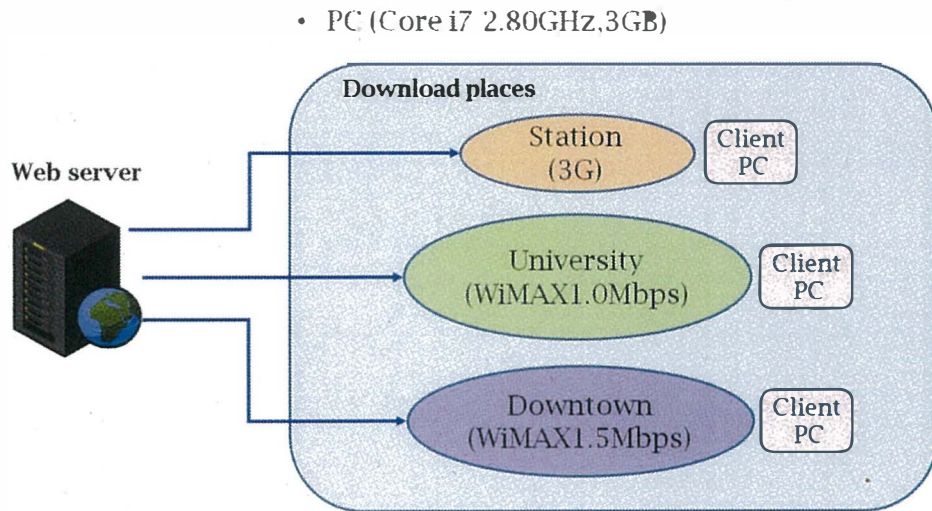


Figure 4.13: Experiment environment.

4.6.1 Evaluation Result by Success Rate

This section describes the success rate of surface fitting method verified by using the actual CAD experimental data. The Table 4.1 below summarizes the number of surfaces whose compression are succeeded and failed. From Table 4.1, we can find that overall success rate of surface fitting is 92.0(%), proposed method is effective and useful.

Table 4.1: Success rate of surface fitting.

	<i>The total number of surfaces (No.)</i>	<i>Success (No.)</i>	<i>Failure (No.)</i>	<i>Success rate(%)</i>
A	24900	22712	2188	91.2(%)
B	24028	22554	1474	93.9(%)
C	6399	5518	881	86.2(%)
D	7204	7036	168	97.7(%)
E	5061	4651	410	91.9(%)
F	1659	1586	73	95.6(%)
G	1560	1345	215	86.2(%)
H	3252	2704	548	83.1(%)
Total	74063	68106	5957	92.0(%)

4.6.2 Evaluation Result by Data Size

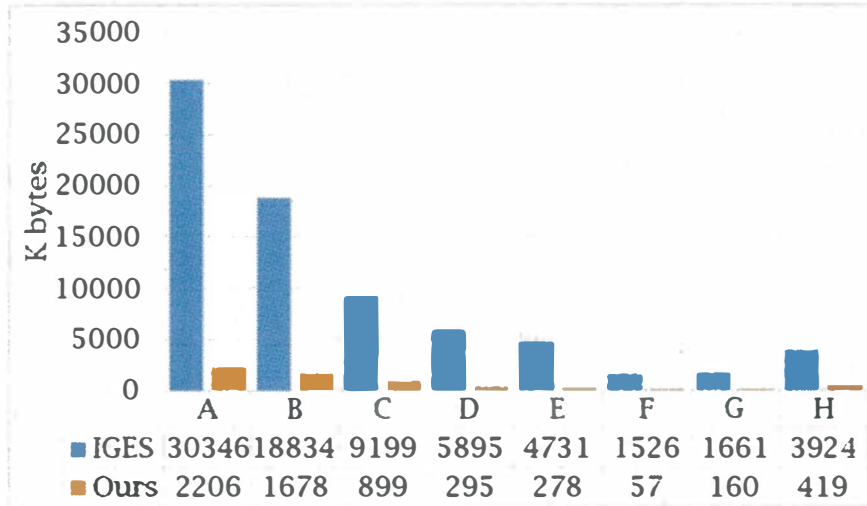
This section describes our evaluation result by data size of the experiment CAD data. In Figure 4.14, data from A to H represent the practical CAD data used in our experiment. The size of three kinds of data, IGES data compressed in the Zip format, commercial software data and our compressed data to which our method is applied are compared for performance evaluation. As shown in Figure 4.14(a), blue bars represent IGES data and orange ones represent our data. In Figure 4.14(b), purple bars represent commercial software data and orange ones represent our data. We can find that the data size is significantly

reduced by using our proposed compression method. For instance, in data F, the size of our data is approximately 26.7 times smaller than that of the IGES data. And also in data F, the size of our data is approximately 1.4 times smaller than that of the commercial software data.

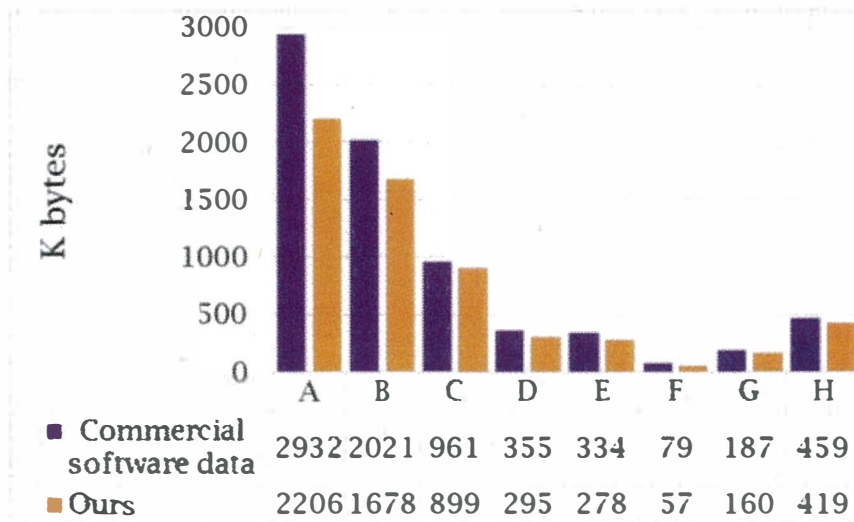
Moreover, we evaluated performance of our data compression method with the different set of tolerance values. In Table 4.2, the experimental data from A to D, is compared with different tolerance values (we employed 10, 1, and 0.1 (%)). In this thesis, when ratio of the bounding box size and the maximum distance between source surface and generated surface is smaller than 1%, it is assumed that the surface is approximated in good accuracy [7]. Since our method is based on fitting a shape with information on tangent planes and boundary edges of the surface [7], it is apparent that significant surface can be generated even by increasing the tolerance. In addition, since the change of tolerance does not contribute significantly to compression, it is necessary to increase the pattern to be successful in the surface fitting. If the pattern increase, the compression ratio will be increase. Increase of the pattern is a topic for our future research.

Table 4.2: Comparison of data size (KB) with different tolerance values (%).

<i>Tolerance</i> (%)	A	B	C	D
10	1,819	1,648	768	292
1	2,206	1,678	899	295
0.1	2,597	1,792	915	306



(a)



(b)

Figure 4.14: Comparison of data size.

4.6.3 Evaluation Result by Data Transmission Time

This section describes our evaluation result by data transmission time of the experiment CAD data, and why it is necessary to actually measure the data transmission time rather than just use the theoretical value. Firstly, the download time for both IGES data compressed with the ZIP format and our compressed data to which our method is applied are compared for the 3G and WiMAX environments. The theoretical value of the maximum possible data speed around 300kbps (download) [38] and 40Mbps (download) [39] are used for 3G and WiMAX environments respectively. Tables 4.3 and 4.4 show the difference of download time of IGES data in 3G environment, and Tables 4.5 and 4.6 show in WiMAX environment. We can see from the tables, the actual measured download time is slower than the theoretical value. Broadband speeds are theoretical maximums which the ideal state for use all the bandwidth. However, in practice such use is not assumed, actual speed achieved varies depending on factors such as your location, equipment capabilities, software, source of your download and volume of network traffic. Because the more people using broadband at the same exchange, the lower the speed will be. Therefore, it is necessary to adjust the parameters of the transfer and retrieval to fit the measured values. Theoretical value is for reference only, not be used for the parameter tuning. It is necessary to actually measure the data transmission time in order to evaluate our transmission system.

Secondly, by using the method described in section 4.6, we evaluated our transmission system by actually measuring the download time and retrieval time of compressed IGES data and our data with 3G, WiMAX 1.0Mbps and WiMAX 1.5Mbps. The unit of time is second. As shown in Tables 4.7 and 4.8, the data transmission time of IGES data and our data is compared. Figure 4.15 shows the graphs of Table 4.7 and Table 4.8. The green bars represent the download time and the red ones represent the retrieval time. Even though the retrieval time of our data is slower than the download time, overall performance of our data is faster than the IGES data. For example, in data F, the transmission time of our data is approximately 39 times faster than that of the IGES data in 3G environments, approximately 10 times faster with WiMAX 1.0Mbps, and approximately 8 times faster than IGES data with WiMAX 1.5Mbps.

Table 4.3: Comparison of the theoretical and experimental values : difference of download time for IGES data in 3G environment.

<i>IGES data (3G)</i>	A	B	C	D	E	F	G	H
<i>Data size (KB)</i>	30346	18834	9199	5895	4731	1526	1661	3924
<i>Theoretical Value (sec.)</i>	809	502	245	157	126	41	44	105
<i>Experimental Value (sec.)</i>	1350	890	650	324	230	164	159	121
<i>Difference (sec.)</i>	-659	-422	-405	-167	-104	-123	-115	-16

Table 4.4: Comparison of the theoretical and experimental values : difference of download time for Our data in 3G environment.

<i>Our data (3G)</i>	A	B	C	D	E	F	G	H
<i>Data size (KB)</i>	2206	1678	899	295	278	57	160	419
<i>Theoretical Value (sec.)</i>	59	45	24	8	7	1.5	4	11
<i>Experimental Value (sec.)</i>	111	57	44	32	11	2	5	38
<i>Difference (sec.)</i>	-52	-12	-20	-24	-6	-0.5	-1	-27

Table 4.5: Comparison of theoretical and experimental values : difference of download time for IGES data in WiMAX environment.

<i>IGES data (WiMAX)</i>	A	B	C	D	E	F	G	H
<i>Data size (KB)</i>	30346	18834	9199	5895	4731	1526	1661	3924
<i>Theoretical Value (sec.)</i>	6	4	2	1.2	0.9	0.3	0.3	0.8
<i>Experimental Value (sec.)</i>	602	359	150	112	50	23	27	77
<i>Difference (sec.)</i>	-596	-355	-148	-110.8	-49.1	-22.7	-26.7	-76.2

Table 4.6: Comparison of theoretical and experimental values : difference of download time for Our data with WiMAX environment.

<i>Our data (WiMAX)</i>	A	B	C	D	E	F	G	H
<i>Data size (KB)</i>	2206	1678	899	295	278	57	160	419
<i>Theoretical Value (sec.)</i>	0.4	0.3	0.2	0.05	0.05	0.01	0.03	0.08
<i>Experimental Value (sec.)</i>	36	13	15	4	1	1	1	3
<i>Difference (sec.)</i>	-35.6	-12.7	-14.8	-3.95	-0.95	-0.99	-0.97	-2.92

4.7 Summary

In this thesis, we evaluated the compression and retrieval method by applying it to 3D surface models based on the curve mesh interpolation method and N-side filling method. Time of compression depends on data size only. The transmission time depends on data size and transmission speed. Since our method achieved high level compression, our method has advantages with big data and in low-speed network environment. We verified effectiveness of our method with practical data. As a result, despite of the different terminal speeds of network environment, our system can exchange gigantic data to a smaller size in a shorter time.

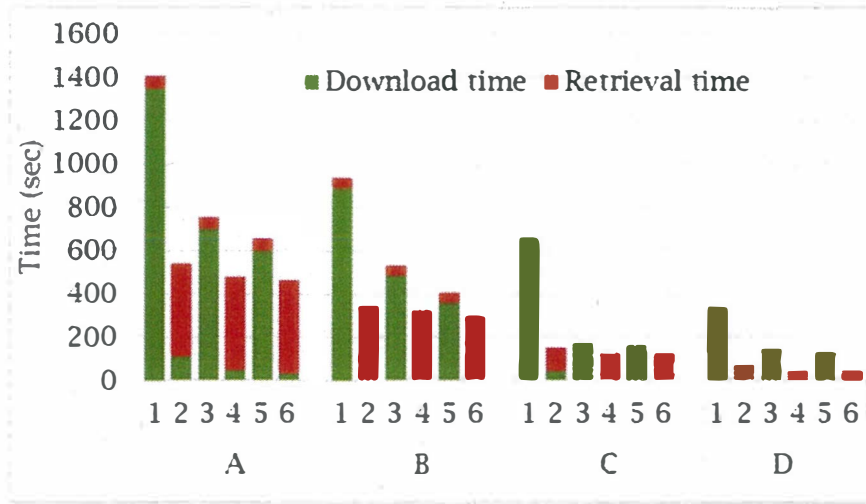
As described in section 4.4, the data size and calculation cost for surface retrieval are antinomy in each other, it is necessary to consider the balance of the data size and the retrieval time.

Table 4.7: Total display time for IGES data.

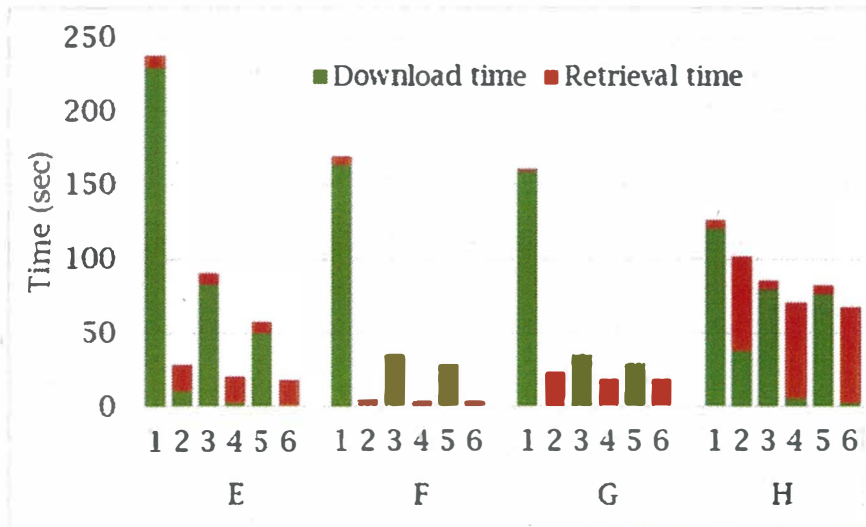
<i>IGES data</i>	<i>Retrieval time (sec.)</i>	<i>Download time (sec.) (3G)</i>	<i>Display time (sec)</i>	<i>Download time(sec.) (WiMAX 1.0Mbps)</i>	<i>Display time (sec.)</i>	<i>Download time(sec.) (WiMAX 1.5Mbps)</i>	<i>Display time (sec.)</i>
A	54.81	1,350	1404.81	700	754.81	602	656.81
B	45.78	890	935.78	484	529.78	359	404.78
C	11.92	650	661.92	163	174.92	150	161.92
D	17.84	324	341.84	128	145.84	112	129.84
E	7.13	230	237.13	83	90.13	50	57.13
F	5.24	164	169.24	30	35.24	23	28.24
G	2.45	159	161.45	33	35.45	27	29.45
H	4.59	121	125.59	80	84.59	77	81.59

Table 4.8: Total display time for our data.

<i>Our data</i>	<i>Retrieval time (sec.)</i>	<i>Download time (sec.) (3G)</i>	<i>Display time (sec.)</i>	<i>Download time(sec.) (WiMAX 1.0Mbps)</i>	<i>Display time (sec.)</i>	<i>Download time(sec.) (WiMAX 1.5Mbps)</i>	<i>Display time (sec.)</i>
A	427.22	111	538.22	53	480.22	36	463.22
B	285.7	57	342.7	38	323.7	13	299.48
C	109.86	44	153.86	19	128.86	15	125.08
D	40.84	32	72.84	5	45.84	4	44.98
E	16.81	11	27.81	3	19.81	1	17.95
F	2.39	2	4.39	1	3.39	1	3.39
G	17.97	5	22.97	1	18.97	1	19.03
H	63.94	38	101.94	6	69.94	3	67.07



(a)



(b)

Figure 4.15: (a) and (b) show comparison of data transmission time for IGES data and ours, odd numbers represent IGES data and even ones represent our data. Pairs of 1 & 2, 3 & 4, and 5 & 6 are the results of transmission time for 3G, WiMAX 1.0Mbps and WiMAX 1.5Mbps respectively.

Chapter 5

Conclusion and Future Work

5.1 Conclusion

The goal of this work was to make contribution to the communication among downstream processes using 3D data. To be more concrete, first we proposed a new surface representation to solve the problems of the Muraki's method, then, contributed to the development of the current 3D data compression and retrieval method and evaluated the 3D data compression and retrieval application system with different network environments: such as third generation of mobile telecommunications (3G) and Worldwide Interoperability for Microwave Access (WiMAX). In this section, our main contribution can be summarized as follow:

- as described in chapter 3, we have proposed the method of generating a smooth surface with a hole that connects to adjacent surfaces with G^1 -continuity by applying our new surface representation to a closed region. The proposed method integrates the advantages of the Gregory and B-spline surfaces. Concretely, the inner control points are obtained based on least squares approximation method, and the G^1 -continuous control points on the boundary are obtained from the joining equations as described in section 3.5. Moreover, our method is independent of the position and the hole shape. Our method is also applicable to a region surrounded by surfaces in all directions connecting with G^1 -continuity. Since our method generates a surface from boundary edge information,

it is applicable to various applications. For instance, by including our method in the trimmed surface compression method [6, 25], a smooth surface with good quality can be generated. It is also effective for direct modeling where shapes with a hole are modified.

- as described in chapter 4, we evaluated the compression and retrieval method by applying it to 3D surface models based on the curve mesh interpolation method and N-side filling method. Time of compression depends on data size only. The transmission time depends on data size and transmission speed. Since our method achieved high level compression, our method has advantages with big data and in low-speed network environment. We verified effectiveness of our method with practical data. As a result, despite of the different terminal speeds of network environment, our system can exchange gigantic data to a smaller size in a shorter time.

5.2 Future Work

This section describes our future works and following things must be improved in order to improve and overcome the obstacles along the way to communicate with 3D models designed with 3D CAD systems.

- In our new surface fitting method, by integrating the Gregory and B-spline surfaces, a smooth surface is generated in good accuracy for a downstream process as a reference model. Therefore, it is necessary to implement the new surface representation. In this thesis, on a common boundary where two surfaces are connected with G^1 -continuity, an input curve mesh is represented by cubic Bézier curves and the G^1 -continuous control points on the boundary are obtained from the joining equations. Therefore, it is necessary to extend our method so that it can be applied to shapes with complex composite boundary curves or B-spline curves with multiple segments.
- In our experiment, our method is only applied to the shapes with a hole as described in section 3.6. Therefore, it is necessary to improve our method so that it can be applicable to the shapes with multiple

holes. Moreover, in our method knots were inserted only at parameters $(u_0 = 0.5, v_0 = 0.5)$ in order to prevent the occurrence of micro knots, when merging the two B-spline surfaces. Therefore, it is our future research topic to increase the internal knots in order to improve the surface accuracy.

- Iterative approximation process is one of the options in the future works, in order to improve generated surface accuracy. In our future works, it is even better adjacent surfaces are take into consideration, in order to get a better result.
- Since the data size and calculation cost for surface retrieval are antinomy in each other as described in section 4.4, it is necessary to consider the balance of the data size and the retrieval time in the future work. As described in section 4.6.2, since the pattern to be successful in the surface fitting has contribution to the compression ratio, it is our future research topic to increase the pattern to be successful in the surface fitting.

Appendix A

Derivation of the joining equations

In order for two surfaces \mathbf{S}^1 and \mathbf{S}^2 , shown in Figure 3.2(a) with a common boundary curve to have a G^1 -continuity, the derivative vectors on the boundary curves should satisfy the condition defined by Equation (3.7). When $v = 0$ and $v = 1$ are assigned to Equations (3.7) and (A.1) is obtained.

$$\begin{aligned} \mathbf{b}_0 &= k_0 \mathbf{a}_0 + h_0 \mathbf{c}_0 \\ \mathbf{b}_3 &= k_1 \mathbf{a}_3 + h_1 \mathbf{c}_2 \end{aligned} \tag{A.1}$$

Let \mathbf{a}_0^3 be the vector between control points of Bézier boundary curve \mathbf{a}_0 and \mathbf{b}_0 , \mathbf{a}_3^3 be the vector between control points of Bézier boundary curve \mathbf{a}_3 and \mathbf{b}_3 . Vectors $\mathbf{a}_1^3, \mathbf{a}_2^3$ are obtained by Equation (A.2).

$$\begin{aligned} \mathbf{a}_0^3 &= \frac{\mathbf{a}_0 + \mathbf{b}_0}{|\mathbf{a}_0 + \mathbf{b}_0|} \\ \mathbf{a}_1^3 &= \frac{2\mathbf{a}_0^3 + \mathbf{a}_3^3}{3} \\ \mathbf{a}_2^3 &= \frac{\mathbf{a}_0^3 + 2\mathbf{a}_3^3}{3} \\ \mathbf{a}_3^3 &= \frac{\mathbf{a}_3 + \mathbf{b}_3}{|\mathbf{a}_3 + \mathbf{b}_3|} \end{aligned} \tag{A.2}$$

Here, to satisfy Equation (A.1), the scalar functions $k(v)$ and $h(v)$ about v are assumed to be linear functions. From Equations (3.7) and (3.8), the

Equation (A.3) is obtained using the vectors between the control points of the surface (See Figure 3.2(b)). Where, $B_i^3(v)$ is Bernstein base polynomial [1].

$$\begin{aligned} \sum_{i=0}^3 B_i^3(v) \mathbf{b}_i = & \{k_0(1-v) + k_1v\} \sum_{i=0}^2 B_i^2(v) \mathbf{a}_i^2 \\ & + \{(1-v)h_0 + vh_1\} \sum_{i=0}^2 B_i^2(v) \mathbf{c}_i \end{aligned} \quad (\text{A.3})$$

Since the left side of the Equation (A.3) is cubic, the degree of polynomial \mathbf{a}_i^2 is limited to quadratic. Therefore, when we assume \mathbf{a}_i^2 using Equation (A.3), \mathbf{a}_i^2 is calculated using Equation (A.4).

$$\begin{aligned} \mathbf{a}_0^2 &= \mathbf{a}_0^3 \\ \mathbf{a}_1^2 &= \frac{3\mathbf{a}_1^3 - \mathbf{a}_0^3}{2} = \frac{3\mathbf{a}_2^3 - \mathbf{a}_3^3}{2} \\ \mathbf{a}_2^2 &= \mathbf{a}_3^3 \end{aligned} \quad (\text{A.4})$$

The control vectors \mathbf{b}_1 and \mathbf{b}_2 can be derived from Equations (3.7), (3.8) and (A.3).

$$\begin{aligned} \mathbf{b}_1 &= \frac{(k_1 - k_0)\mathbf{a}_1^3}{3} + k_0\mathbf{a}_1^3 + \frac{2h_0\mathbf{c}_1}{3} + \frac{h_1\mathbf{c}_0}{3} \\ \mathbf{b}_2 &= k_1\mathbf{a}_2^3 - \frac{(k_1 - k_0)\mathbf{a}_3^3}{3} + \frac{h_0\mathbf{c}_2}{3} + \frac{2h_1\mathbf{c}_1}{3} \end{aligned} \quad (\text{A.5})$$

Appendix B

Surface inner control point calculation by least-squares approximation method

In Figure 4.1, unknown control points are calculated by using the least-squares approximation method [21]. When the fitting Gregory patch is $\mathbf{S}(u, v)$, the surface control points are $\mathbf{Q}_{i,j}$ ($0 \leq i \leq n, 0 \leq j \leq m$). Surface $\mathbf{S}(u, v)$ is expressed by Equation (B.1).

$$\mathbf{S}(u, v) = \sum_{i=0}^n \sum_{j=0}^m N_{i,k}(u) N_{j,k}(v) \mathbf{Q}_{i,j} \quad (\text{B.1})$$

where $n = 4, m = 4$ and $k = 3$. The $t + 1$ sample points on hole area are assumed to be \mathbf{Q}_s ($0 \leq s \leq t$) and the parameters of u and v directions are assumed to be \bar{u}_s and \bar{v}_s . Surface $\mathbf{S}(u, v)$ is calculated so that the square sum of the distances between the sample points \mathbf{Q}_s and corresponding points $\mathbf{S}(\bar{u}_s, \bar{v}_s)$ on the surface is minimized. Then, Equation (B.2) is obtained.

$$f = \sum_{s=0}^t |\mathbf{Q}_s - \mathbf{S}(\bar{u}_s, \bar{v}_s)|^2 \quad (\text{B.2})$$

APPENDIX B. SURFACE INNER CONTROL POINT CALCULATION
BY LEAST-SQUARES APPROXIMATION METHOD

In Equation (B.1), the control point showing the boundary curve is already known. When the known control point is assumed to be \mathbf{R}_s , Equation (B.4) is obtained.

$$\begin{aligned}
\mathbf{R}_s = & \mathbf{Q}_s - (N_{0,k}(\bar{u}_s)N_{0,k}(\bar{v}_s)\mathbf{P}_{0,0} + \dots + N_{0,k}(\bar{u}_s)N_{0,k}(\bar{v}_s)\mathbf{P}_{0,m} \\
& + N_{1,k}(\bar{u}_s)N_{0,k}(\bar{v}_s)\mathbf{P}_{1,0} + \dots + N_{n-1,k}(\bar{u}_s)N_{0,k}(\bar{v}_s)\mathbf{P}_{n-1,0} \\
& + N_{1,k}(\bar{u}_s)N_{m,k}(\bar{v}_s)\mathbf{P}_{1,m} + \dots + N_{n-1,k}(\bar{u}_s)N_{m,k}(\bar{v}_s)\mathbf{P}_{n-1,m} \\
& + N_{n-3,k}(\bar{u}_s)N_{m-1,k}(\bar{v}_s)\mathbf{P}_{n-3,m-1} + N_{n-2,k}(\bar{u}_s)N_{m-1,k}(\bar{v}_s)\mathbf{P}_{n-2,m-1} \\
& + N_{n-3,k}(\bar{u}_s)N_{1,k}(\bar{v}_s)\mathbf{P}_{n-3,1} + N_{n-2,k}(\bar{u}_s)N_{1,k}(\bar{v}_s)\mathbf{P}_{n-2,1} \\
& + N_{n-1,k}(\bar{u}_s)N_{1,k}(\bar{v}_s)\mathbf{P}_{n-1,1} + \dots + N_{n-1,k}(\bar{u}_s)N_{m-1,k}(\bar{v}_s)\mathbf{P}_{n-1,m-1} \\
& + N_{1,k}(\bar{u}_s)N_{1,k}(\bar{v}_s)\mathbf{P}_{1,1} + \dots + N_{1,k}(\bar{u}_s)N_{m-1,k}(\bar{v}_s)\mathbf{P}_{1,m-4} \\
& + N_{n,k}(\bar{u}_s)N_{0,k}(\bar{v}_s)\mathbf{P}_{n,0} + \dots + N_{n,k}(\bar{u}_s)N_{m,k}(\bar{v}_s)\mathbf{P}_{n,m})
\end{aligned} \tag{B.3}$$

$$\begin{aligned}
f = & \sum_{s=0}^t |\mathbf{Q}_s - \mathbf{S}(\bar{u}_s, \bar{v}_s)|^2 \\
= & \sum_{s=0}^t \left[\mathbf{R}_s \cdot \mathbf{R}_s - 2 \sum_{i=2}^{n-2} \sum_{j=2}^{m-2} B_{i,k}(\bar{u}_s)N_{j,k}(\bar{v}_s)(\mathbf{R}_s \cdot \mathbf{P}_{i,j}) \right. \\
& \left. + \left(\sum_{i=2}^{n-2} \sum_{j=2}^{m-2} N_{i,k}(\bar{u}_s)N_{j,k}(\bar{v}_s)\mathbf{P}_{i,j} \right) \cdot \right. \\
& \left. \left(\sum_{i=2}^{n-2} \sum_{j=2}^{m-2} N_{i,k}(\bar{u}_s)N_{j,k}(\bar{v}_s)\mathbf{P}_{i,j} \right) \right]
\end{aligned} \tag{B.4}$$

If Equation (B.4) is differentiated by unknown control point $\mathbf{P}_{\alpha,\beta}$ and the differentiation value becomes 0, the value of f is minimized.

$$\frac{\partial f}{\partial \mathbf{P}_{\alpha,\beta}} = 0 \tag{B.5}$$

where $2 \leq \alpha \leq n-2$ and $2 \leq \beta \leq m-2$. From Equations (B.4) and (B.5), Equation (B.6) is obtained.

APPENDIX B. SURFACE INNER CONTROL POINT CALCULATION
BY LEAST-SQUARES APPROXIMATION METHOD

$$\begin{aligned} \sum_{i=2}^{n-2} \sum_{j=2}^{m-2} \left(\sum_{s=0}^t N_{\alpha,k}(\bar{u}_s) N_{\beta,k}(\bar{v}_s) N_{i,k}(\bar{u}_s) N_{j,k}(\bar{v}_s) \right) \mathbf{P}_{i,j} \\ = \sum_{s=0}^t N_{\alpha,k}(\bar{u}_s) N_{\beta,k}(\bar{v}_s) \mathbf{R}_s \end{aligned} \quad (\text{B.6})$$

When $(n-3) \times (m-3)$ Equations are set up for $\mathbf{P}_{\alpha,\beta}$ ($2 \leq \alpha \leq n-2, 2 \leq \beta \leq m-2$) of Equation (B.6), the following matrix is obtained.

$$\mathbf{NP} = \mathbf{R} \quad (\text{B.7})$$

where

$$\mathbf{N} = \begin{bmatrix} \mathbf{A}_{2,2,i,j} \\ \vdots \\ \mathbf{A}_{\alpha,\beta,i,j} \\ \vdots \\ \mathbf{A}_{n-2,m-2,i,j} \end{bmatrix} \quad (\text{B.8})$$

$$\begin{aligned} \mathbf{A}_{2,2,i,j} = & \left[\begin{aligned} & \sum_{s=0}^t N_{2,k}(\bar{u}_s) N_{2,k}(\bar{v}_s) N_{2,k}(\bar{u}_s) N_{2,k}(\bar{v}_s), \dots, \\ & \sum_{s=0}^t N_{2,k}(\bar{u}_s) N_{2,k}(\bar{v}_s) N_{i,k}(\bar{u}_s) N_{j,k}(\bar{v}_s), \dots, \\ & \sum_{s=0}^t N_{2,k}(\bar{u}_s) N_{2,k}(\bar{v}_s) N_{n-2,k}(\bar{u}_s) N_{m-2,k}(\bar{v}_s) \end{aligned} \right] \end{aligned} \quad (\text{B.9})$$

$$\begin{aligned} \mathbf{A}_{\alpha,\beta,i,j} = & \left[\begin{aligned} & \sum_{s=0}^t N_{\alpha,k}(\bar{u}_s) N_{\beta,k}(\bar{v}_s) N_{2,k}(\bar{u}_s) N_{2,k}(\bar{v}_s), \dots, \\ & \sum_{s=0}^t N_{\alpha,k}(\bar{u}_s) N_{\beta,k}(\bar{v}_s) N_{i,k}(\bar{u}_s) N_{j,k}(\bar{v}_s), \dots, \\ & \sum_{s=0}^t N_{\alpha,k}(\bar{u}_s) N_{\beta,k}(\bar{v}_s) N_{n-2,k}(\bar{u}_s) N_{m-2,k}(\bar{v}_s) \end{aligned} \right] \end{aligned} \quad (\text{B.10})$$

APPENDIX B. SURFACE INNER CONTROL POINT CALCULATION
BY LEAST-SQUARES APPROXIMATION METHOD

$$\mathbf{R} = \begin{bmatrix} N_{2,k}(\bar{u}_0)N_{2,k}(\bar{v}_0)\mathbf{R}_0 + \cdots + N_{2,k}(\bar{u}_t)N_{2,k}(\bar{v}_t)\mathbf{R}_t \\ \vdots \\ N_{n-2,k}(\bar{u}_0)N_{n-2,k}(\bar{v}_0)\mathbf{R}_0 + \cdots + N_{n-2,k}(\bar{u}_t)N_{n-2,k}(\bar{v}_t)\mathbf{R}_t \end{bmatrix} \quad (\text{B.11})$$

$$\mathbf{P} = \begin{bmatrix} \mathbf{P}_{2,2} \\ \vdots \\ \mathbf{P}_{n-2,m-2} \end{bmatrix} \quad (\text{B.12})$$

Solving Equation (B.7) obtains unknown control points $\mathbf{P}_{i,j}$.

Bibliography

- [1] C. Jackson, D. Prawel, P. Brown: *The 2013 State of 3D Collaboration and Interoperability Report*, Published by: Life Cycle Insight & Long View Advisors, (2013)
- [2] D. J. Kasik, W. Buxton, D. R. Ferguson: *Ten CAD model challenges*, IEEE Computer Graphics and Applications, Vol.25, No.2, pp.81-92, (2005)
- [3] G. Farin: *Curves and Surfaces for Computer Aided Geometric Design A Practical Guide*, Academic Press, (2002)
- [4] Y. Muraki, K. Konno, Y. Tokuyama: *A Study of Subdivision Method to Three and Five Sided Faces Based on Regular Polygon*, in Proc. of IWAIT 2009, (2009)
- [5] Muraki, Y.; Matsuyama, K.; Konno, K. Tokuyama, Y.: *A Study of Surface fitting Method of an N-sided Region Considering G^1 -Continuity with Adjacent Surfaces*, in Proceedings of IWAIT (2012)
- [6] Y. Muraki, K. Matsuyama, K. Konno, Y. Tokuyama: *Data Compression Method for Trimmed Surfaces Based on Surface Fitting with Maintaining G^1 -Continuity with Adjacent Surfaces*, Computer Aided Design and Applications, Vol.9, No.6, pp.811-824, (2012)

- [7] Y. Muraki, K. Matsuyama, K. Konno, Y. Tokuyama: *Reconstruction Method of Trimmed Surfaces with Maintaining G^1 -continuity with Adjacent Surfaces*, Computer Aided Design and Applications, Vol.11, No.2, pp.165-171, (2014)
- [8] E. Catmull, J. Clark *Recursively generated B-spline surfaces on arbitrary topological meshes*, Computer Aided Design, Vol. 10, No. 6, pp. 350-355, (1978)
- [9] L. Piegl, W. Tiller: *Filling n-sided regions with NURBS patches*, The Visual Computer, Vol. 2, No. 15, pp. 77-89, (1999)
- [10] Yi-Jun. Yang, Jun-Hai. Yong, Hui. Zhang, Jean-Claude. Paul, Jia-Guang. Sun: *A rational extension of Piegl's method for filling n-sided holes*, Computer Aided Design, Vol. 38, No. 11, pp. 1166-1178, (2006)
- [11] N. Pla-Garcia, M. Vigo-Anglada, J. Cotrina-Navau: *N-sided patches with B-spline boundaries*, Computers & Graphics, Vol. 30, No. 6, pp. 959-970, (2006)
- [12] Y. Muraki, K. Konno, Y. Tokuyama: *Curve Mesh Modeling Method of Trimmed Surfaces for Direct Modeling*, The Journal of Art and Science, Vol. 10, No. 1, pp. 12-27, (2011)
- [13] H. Chiyokura , F. Kimura : *Design of Solids with free-form surfaces*, Computer & Graphics (Pro.SIGGRAPH 83) Vol.17, No.3, pp.289-298,(1983)
- [14] K. Konno, H. Chiyokura: *An Approach of Designing and Controlling Free-Form Surfaces by Using NURBS Boundary Gregory Patches*, Computer Aided Geometric Design, Vol.13, No.9, pp.825-849,(1996)

- [15] Y. Tokuyama, K. Konno: *Filling N-sided Region with a B-spline Surface*, Information Processing Society of Japan, Vol. 43, No. 10, pp. 3209-3218, (2002)
- [16] G. W. Mu, T. Zang, S. J. Dai,: *Surface Reconstruction via Interpolating Boundary Curves and Cross-Boundary Derivatives Simultaneously Approximating Inner Points*, Applied Mechanics and Materials, Vols. 321-324, pp. 1821-1826, (2013)
- [17] T. W. Sederberg, D. L. Cardon, G. T. Finnigan, N. S. North, J. Zheng, and T. Lyche: *T-spline Simplification and Local Refinement*, SIGGRAPH 2004, Vol. 23, No. 3, pp. 276-283, (2004)
- [18] T. W. Sederberg, J. Zheng, A. Bakenov, and A. Narsri: *T-splines and T-NURCCs*, ACM Transactions on Graphics, Vol. 23, No. 3, pp. 477-484, (2003)
- [19] ISO 10303-59:2008 Industrial automation systems and integration, *Product data representation and exchange, Part 59: Integrated generic resource, Quality of product shape data*, International Organization for Standardization.
- [20] C. Deng, X. Yang *A simple method for interpolating meshes of arbitrary topology by Catmull-Clark surfaces*, The Visual Computer, Vol. 26, No. 2, pp. 137-146, (2009)
- [21] L. Piegl, W. Tiller: *The NURBS Book*, Springer-Verlag, (1995)
- [22] K. Konno, Y. Tokuyama, H. Chiyokura: *A G^1 connection around complicated curve meshes using G^1 NURBS Boundary Gregory Patches*, Computer Aided Design, Vol. 33, No. 4, pp. 293-306, (2001)

- [23] H. Toriya, H. Chiyokura: *3D CAD: Principles and Applications (Computer Science Workbench)*, Springer-Verlag, New York, Berlin, Tokyo, (1993)
- [24] A. Wakita, M. Yajima, T. Harada, H. Toriya, H. Chiyokura: *XVL: A Compact and Qualified 3D Representation With Lattice Mesh and Surface for the Internet*, in Proceedings of the Web3D-VRML 2000 fifth symposium on 3D Web technology, Monterey, California, February, 2000, 21-24, ACM-Press.
- [25] G. Silayi, T. Kinoshita, Y. Muraki, K. Matsuyama, K. Konno: *Evaluation of 3D Data Compression and Retrieval Method Based on Curve Mesh Filling*, Computer Aided Design and Applications, Vol. 12, No. 5, pp. 546-554, (2015)
- [26] H. Toriya, H. Chiyokura: *Basics and Applications of Three-dimensional CAD*, Kyoritsu Shuppan Co., Ltd., (1991)
- [27] T. W. Sederberg, J. Zheng, A. Bakenov, and A. Narsri: *T-splines and T-NURCCs*, ACM Transactions on Graphics, Vol. 23, No. 3, pp. 477-484, (2003)
- [28] Y. Tokuyama, K. Konno: *Reparameterization of piecewise rational Bézier curves and its applications*, The Visual Computer, Vol. 17, No.6, pp. 329-336, (2001).
- [29] K. Konno, H. Chiyokura: *G^1 and G^1 Surface Interpolation over Curve Meshes and Its Shape Control*, International Journal of SHAPE MODELING, Vol. 2, No 1, pp. 1-20, (1996)
- [30] Beeker, E.: *Smoothing of shapes designed with free-form surfaces*, Computer-Aided Design, Vol.18, No.4, pp. 224-232, (1986)

- [31] Coons, S.-A.: *Surface patches and B-spline curves*, in *Computer Aided Geometric Design* (Barnhill, R.-E. and Riesenfeld, R.-F. Eds.), Academic Press, New York, (1974)
- [32] Du, W.-H.; Schmitt, F.-J.-M.: *On the G^1 continuity of piecewise Bézier surfaces: a review with new results*, *Computer-Aided Design*, Vol.22, No.9, pp. 556-573, (1990)
- [33] Hoschek, J.; Schneider, F.; Wassum, P.: *Optimal approximate conversion of spline surfaces*, *Computer-Aided Geometric Design*, Vol.6, No.4, pp. 293-306, (1989)
- [34] Hoschek, J.; Lasser, D.: *Fundamentals of Computer Aided Geometric Design*, AK Peters, Wellesley, MA (1993)
- [35] Lee, K.: *Principles of CAD/CAM/CAE Systems*, Addison-Wesley, (1999)
- [36] Mäntylä, M.: *An Introduction to Solid Modeling*, Computer Science Press, Maryland, (1988)
- [37] web2CAD, <http://www.web2cad.co.jp/>
- [38] <http://www.bmobile.ne.jp/devices/devices.html>
- [39] <http://neet-navi.info/device/wimax/6158/>
- [40] 佐藤直之, 徳山喜政: “微小要素の発生を抑制した複数面のオフセット処理”, *情報処理学会*, Vol.44, No.9, pp.2374-2382, (2003)
- [41] 今野晃市: “曲面メッシュモデリングのための自由曲面間の接続法に関する研究”, *東京大学博士論文*, (1996)

- [42] 今野晃市, 千代倉弘明: “NURBS 境界 Gregory パッチによる自由曲面形状の内挿方法”, 情報処理学会論文誌, 第 35 巻, 第 10 号, pp.2203-2213, (1994)
- [43] 今野晃市, 高村禎二, 千代倉弘明: “複合曲線を含んだ不規則な曲線メッシュの内挿方法”, 情報処理学会論文誌, 第 35 巻, 第 6 号, pp. 1211-1221, (1994)
- [44] 今野晃市, 高村禎二, 千代倉弘明: “高品位な自由曲面形状の生成とその形状制御”, 情報処理学会論文誌, 第 33 巻, 第 9 号, pp.1133-1142, (1992)
- [45] 曾根順治, 今野晃市, 千代倉弘明: “NURBS 境界 Gregory パッチによる非四辺形領域への曲面の内挿”, 情報処理学会論文誌, 第 40 巻, 第 2 号, pp. 710-718, (1999)

List of Figures

1.1	The use of 3D Models in downstream processes.	2
1.2	3D Models use off the critical path.	3
1.3	Modifying a boundary edge in direct modeling for data healing.	3
1.4	Example of surface smoothness.	4
2.1	Example of surface interpolation method application to the N-sided area.	8
2.2	The procedure of the N-side filling method.	10
2.3	Problems of the method of Muraki et al.[7].	12
3.1	Concept of our proposed method (b) applied to the gray region of (a).	18
3.2	(a) G^1 -continuity condition and (b) connection of two sur- faces using the joining equations [14].	20
3.3	Inner control point approximation process.	22
3.4	Closed region obtained from CAD.	25
3.5	(a) control points of generated surface A, (b) control points of generated surface B.	26

3.6	(a) control points of generated surface C, (b) control points of generated surface D.	27
3.7	(a) control points of generated surface E, (b) control points of generated surface F.	28
3.8	Control points of generated surface G.	29
3.9	Result of surface evaluation: distances between the generated surface and the source one are calculated. (a) and (b) are the error margins of objects A and C respectively in the Table 3.1.	31
3.10	Result of surface evaluation: distances between the generated surface and the source one are calculated. (a) and (b) are the error margins of objects E and G respectively in the Table 3.1.	32
3.11	Verification of the continuity with adjacent surfaces: the normal vectors of the generated surfaces A and B are coincide with those of the adjacent surfaces on their boundary edges.	33
3.12	Verification of the continuity with adjacent surfaces: the normal vectors of the generated surfaces C and D are coincide with those of the adjacent surfaces on their boundary edges.	34
3.13	Verification of the continuity with adjacent surfaces: the normal vectors of the generated surfaces E and F are coincide with those of the adjacent surfaces on their boundary edges.	35
3.14	Verification of the continuity with adjacent surfaces: the normal vectors of the generated surface G coincide with those of the adjacent surfaces on their boundary edges.	36
4.1	Data compression of 3D data models.	40
4.2	Concept of 3D data compression and retrieval method.	41

4.3	Flow chart of our compression process.	43
4.4	Flow chart of data retrieval process.	45
4.5	Example of surface fitting method application.	46
4.6	Example of surface fitting method application.	47
4.7	Details of surface fitting.	48
4.8	Details of surface fitting.	49
4.9	Example of surface fitting method application.	51
4.10	Example of surface fitting method application.	52
4.11	Example of surface fitting method application.	53
4.12	Evaluation flow for the total time required to display practical data on the screen.	54
4.13	Experiment environment.	54
4.14	Comparison of data size.	57
4.15	(a) and (b) show comparison of data transmission time for IGES data and ours, odd numbers represent IGES data and even ones represent our data. Pairs of 1 & 2, 3 & 4, and 5 & 6 are the results of transmission time for 3G, WiMAX 1.0Mbps and WiMAX 1.5Mbps respectively.	64

List of Tables

3.1	Error evaluation of the source surface and the generated surface.	30
3.2	Difference of error margins around the holes obtained by adding the center point to the sample points.	30
4.1	Success rate of surface fitting.	55
4.2	Comparison of data size (KB) with different tolerance values (%).	56
4.3	Comparison of the theoretical and experimental values : difference of download time for IGES data in 3G environment.	59
4.4	Comparison of the theoretical and experimental values : difference of download time for Our data in 3G environment.	59
4.5	Comparison of theoretical and experimental values : difference of download time for IGES data in WiMAX environment.	60
4.6	Comparison of theoretical and experimental values : difference of download time for Our data with WiMAX environment.	60
4.7	Total display time for IGES data.	62
4.8	Total display time for our data.	63